On the Mechanism of Pacific Multidecadal Climate Variability in CCSM3: The Role of the Subpolar North Pacific Ocean

YAFANG ZHONG AND ZHENGYU LIU

Center for Climatic Research, and Department of Atmospheric and Oceanic Sciences, University of Wisconsin—Madison, Madison, Wisconsin

ABSTRACT

Previous analyses of the Community Climate System Model, version 3 (CCSM3) standard integration have revealed pronounced multidecadal variability in the Pacific climate system. The purpose of the present work is to investigate physical mechanism underlying this Pacific multidecadal variability (PMV). To better isolate the mechanism that selects the long multidecadal time scale for the PMV, a few specifically designed sensitivity experiments are carried out. When the propagating Rossby waves are blocked in the subtropics from the midbasin, the PMV remains outstanding. In contrast, when the Rossby waves are blocked beyond the subtropics across the entire North Pacific, the PMV is virtually suppressed. It suggests that the PMV relies on propagating Rossby waves in the subpolar Pacific, whereas those in the subtropics are not critical.

A novel mechanism of PMV is advanced based on a more comprehensive analysis, which is characterized by a crucial role of the subpolar North Pacific Ocean. The multidecadal ocean temperature and salinity anomalies may originate from the subsurface of the subpolar North Pacific because of the wave adjustment to the preceding basin-scale wind curl forcing. The anomalies then ascend to the surface and are amplified through local temperature–salinity convective feedback. Along the southward Oyashio, these anomalies travel to the Kuroshio Extension (KOE) region and are further intensified through a similar convective feedback. The oceanic temperature anomaly in the KOE is able to feed back to the large-scale atmospheric circulation, inducing a wind curl anomaly over the subpolar North Pacific, which in turn generates anomalous oceanic circulation and causes temperature and salinity variability in the subpolar subsurface. Thereby, a closed loop of PMV is established in the form of an extratropical delayed oscillator. The phase transition of PMV is driven by the delayed negative feedback that resides in the wave adjustment of the subpolar North Pacific via propagating Rossby waves, whereas the convective positive feedback provides the growth mechanism. A significant role of salinity variability is unveiled in both the delayed negative feedback and convective positive feedback.

1. Introduction

Observations have shown evidence of significant Pacific multidecadal variability (PMV) with a time scale of 50–70 yr (Minobe 1997; Mantua et al. 1997; Enfield and Mestas-Nunez 1999; Wu et al. 2003; Deser et al. 2004). However, the mechanism for the PMV has remained poorly understood. Compared to the intensive studies on the mechanisms of the shorter (10–25 yr) Pacific decadal variability (PDV; Latif and Barnett 1994; Minobe 1999, 2000) or the North Atlantic multidecadal variability (Delworth et al. 1993; Enfield and Mestas-Nunez 1999), there has been little study on the mechanism of the PMV. A few recent studies do indicate that the PMV arises from the Pacific Ocean. Through a comprehensive observational analysis, Deser et al. (2004) found a robust multidecadal linkage between the North Pacific and tropical Pacific. They inferred that the PMV originates from the tropical Pacific and then impacts the North Pacific through atmospheric teleconnection. In the Fast Ocean Atmosphere Model (FOAM), a coupled general circulation model (CGCM) based on specifically designed sensitivity experiments, the PMV was explicitly identified to originate in the North Pacific (>20°N; Liu et al. 2002; Wu et al. 2003). In an analysis of a long integration using the ECHAM3/large-scale geostrophic (LSG) CGCM, it was also concluded that the PMV originates in the North Pacific, although the role of active ocean–atmosphere interaction is suggested to be unimportant (Latif 2006).

Corresponding author address: Y. Zhong, CCR, 1225 W. Dayton St., Madison, WI 53706.
E-mail: yafangzhong@wisc.edu

TABLE 1. A list of the sensitivity experiments. Explanations for the PB and PC surgeries are provided in the text.

Case	Expt design
CTRL	Std integration of CCSM3
PC-ET	PC surgery is applied to the tropics equatorward of 20°
BLKNP	PC surgery is applied to the tropics equatorward of 20°; PB surgery is applied to the North Pacific at 10°–60°N
BLKSTP	PC surgery is applied to the tropics equatorward of 20°; PB surgery is applied to the subtropical North Pacific at 10°–35°N

Consistent with the FOAM simulations of Liu et al. (2002) and Wu et al. (2003), Zhong et al. (2008) also identified a North Pacific origin for the PMV in the Community Climate System Model, version 3 (CCSM3). A closer inspection by Zhong et al. (2008) revealed a robust tropical Pacific–North Pacific linkage associated with the North Pacific originated PMV. This model linkage resembles that found in observations (Deser et al. 2004). Because the model PMV is known to arise locally from the North Pacific, it suggests that the diagnostic linkage between the tropical and North Pacific can be consistent with a PMV impact from the North Pacific onto the tropical Pacific. This interpretation of the tropical Pacific–North Pacific linkage thus potentially reconciles the two seemingly contradictory views regarding the origin of PMV.

In spite of previous studies, the mechanism that selects the time scale of the PMV remains unclear. This mechanism is likely to be different from those for the PDV and the North Atlantic multidecadal variability. The time scale of the PDV has been suggested to be associated with the first baroclinic-mode Rossby wave in the midlatitudes (35°–40°N; Seager et al. 2001; Pierce et al. 2001; Schneider et al. 2002; Kwon and Deser 2007; Qiu et al. 2007; d'Orgeville and Peltier 2007) and subtropical (20°–35°N) Pacific (Latif and Barnett 1994, 1996; Kleeman et al. 1999). However, these Rossby waves, which cross the Pacific basin rapidly at interannual to decadal time scales, provide a memory for the PDV but seem too short for the PMV. For the North Atlantic multidecadal variability, an active deep thermohaline circulation is believed to be critical for providing the long multidecadal memory (Delworth et al. 1993; Griffies and Tziperman 1995; Timmermann et al. 1998; Rodwell et al. 1999; Selten et al. 1999; Eden and Greatbatch 2003). However, this mechanism does not apply to the North Pacific, where a similar active thermohaline circulation is absent.

Here, as an extension of Zhong et al. (2008), we further study the fundamental mechanism of PMV. What processes select the multidecadal time scale for PMV?

This is the key question to be addressed. In addition, we also address the potential role of large-scale ocean–atmosphere coupling in the PMV. Sensitivity experiments will be performed by using modeling surgery techniques to isolate the key processes that are responsible for the PMV. Our study suggests that the multidecadal memory of the PMV may reside in the slow westward propagation of the first baroclinic-mode Rossby waves in the subpolar North Pacific Ocean. Furthermore, the subsurface thermocline or halocline variability may affect the surface climate through local convective feedback as well as oceanic advection and interaction with the Kuroshio Extension (KOE). In particular, salinity variability is suggested to provide an indispensable ingredient for both the time-scale selection and convective growth mechanism of PMV. This paper is organized as follows: section 2 introduces the model and the experimental design. A preliminary survey of PMV is undertaken in section 3 for all sensitivity experiments. Section 4 is devoted to depicting the life cycle of the PMV in terms of ocean temperature and salinity evolution. Physical processes driving the life cycle are explored in section 5, which is concluded with a schematic view of PMV. The revealed physics are then substantiated in section 6 with heat and salt budget analyses. Section 7 supplies further discussion on the nature of PMV.

2. Model and experimental design

CCSM3 is a state-of-art global climate model consisting of four components of the atmosphere, ocean, sea ice, and land surface, which are linked through a flux coupler (Collins et al. 2006). We use the version of CCSM3 at T31x3 resolution (Yeager et al. 2006). The atmospheric component is the Community Atmosphere Model version 3 (CAM3) at T31 resolution with 26 levels in the vertical. The ocean model is the Parallel Ocean Program (POP) version 1.4.3 in spherical polar coordinates with a dipole grid and has a nominal horizontal resolution of 3°. The vertical dimension is a depth coordinate with 25 levels extending to 4.75 km. The control simulation (CTRL) is integrated under the present-day climate conditions for 880 yr without flux adjustment. Analyses of CTRL are based on the last 580 yr of simulation.

A series of sensitivity experiments (Table 1) are performed to explore the mechanism of the PMV using the modeling surgery approach of partial coupling (PC) and partial blocking (PB) (Liu et al. 2002; Wu et al. 2003). All experiments were started from the CTRL at year 651 and integrated for 400 yr without flux correction. First, a new control [extratropical run with partial coupling applied in the tropics (PC-ET)] is performed with ocean–atmosphere coupling suppressed in the tropics
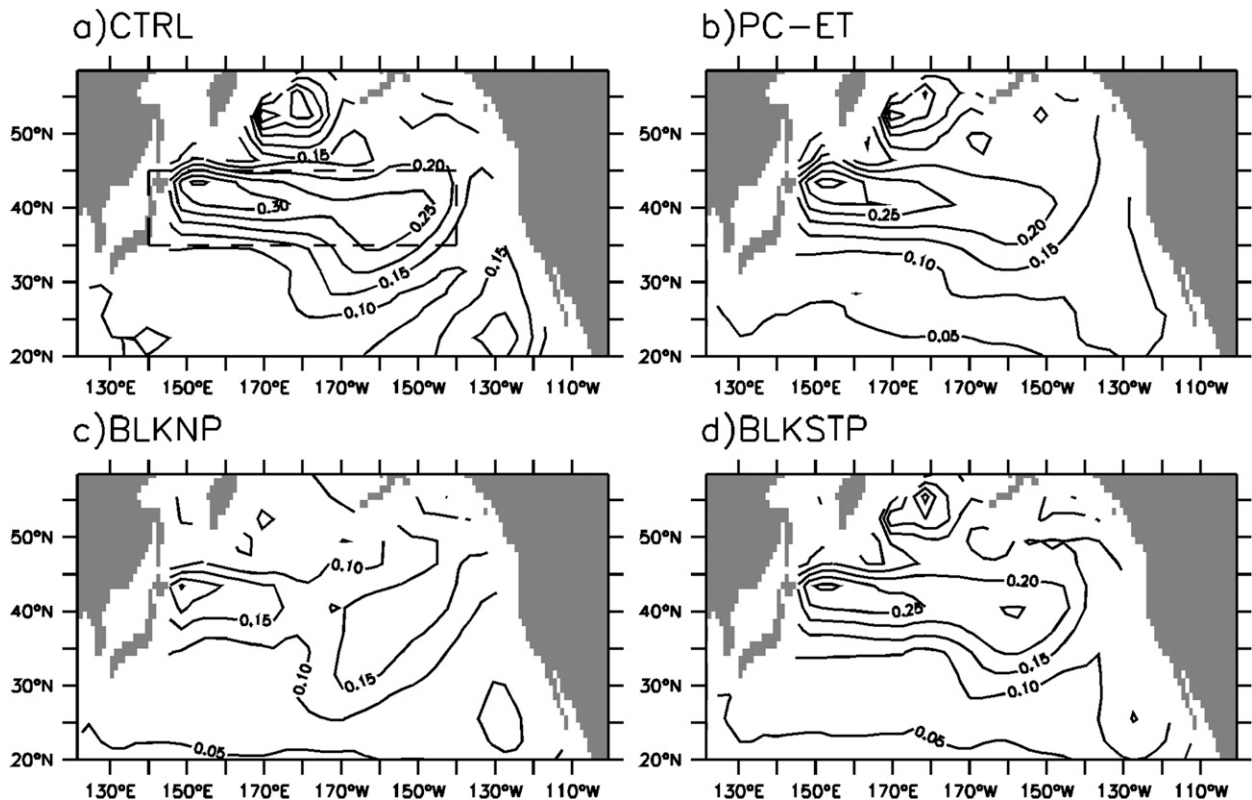
FIG. 1. Spatial distribution of standard deviation of 25–80-yr band-filtered SST in (a) CTRL, (b) PC-ET, (c) BLKNP, and (d) BLKSTP. Contour interval (CI) is 0.05°C. The west-central North Pacific (35°–45°N, 140°E–140°W) is delineated with the dashed rectangular box in (a).

with the PC surgery: equatorward of 20°, the SST to condition the atmosphere is replaced with that of the seasonal cycle of the climatology from CTRL such that the atmosphere sees SST variability only in the extratropics outside of 20°. This new control has been discussed extensively by Zhong et al. (2008; namely, PC-ET). The absence of active ocean–atmosphere coupling in the tropics suppresses coupled tropical climate variability, such as ENSO. Nevertheless, distinguished PMV still takes place in the North Pacific. PC-ET is used to serve as the new base case for additional sensitivity experiments.

To further identify the oceanic mechanism associated with the PMV, two new sensitivity experiments are performed based on PC-ET—with the westward propagation of Rossby waves blocked in the midbasin using the PB surgery by inserting a sponge wall of 10° width (below 100 m) into the ocean model component along the midbasin at longitude of 180°—in which ocean temperature and salinity are restored toward the climatological seasonal cycle of CTRL. In one experiment [namely, partial blocking in the North Pacific (BLKNP)], the sponge wall extends from 10°N to over 60°N such that Rossby wave propagation is blocked in the midbasin across the entire North

Pacific Ocean. In the other experiment [namely, partial blocking in the subtropical North Pacific (BLKSTP)], the sponge wall extends only from 10° to 35°N such that Rossby wave propagation is blocked only in the subtropical ocean. These two PB experiments will help us isolate the roles of Rossby wave propagation in the subtropical and subpolar ocean in the time-scale selection of the PMV.

Unless stated otherwise, all analyses presented here are performed with annual mean data. All time series have been first detrended before further analysis. Standard statistical methods, including lag correlation and regression, band filtering, and spectral analysis, are used. Power spectra are obtained through multitaper spectrum analysis (Mann and Lees 1996).

3. PMV in sensitivity experiments

We first examine the spatial distribution of the variance of multidecadal SST variability in the North Pacific in different experiments (Fig. 1). As discussed before in Zhong et al. (2008), with tropical ocean–atmosphere coupling suppressed, the multidecadal variability in PC-ET (Fig. 1b) remains similar to CTRL (Fig. 1a),
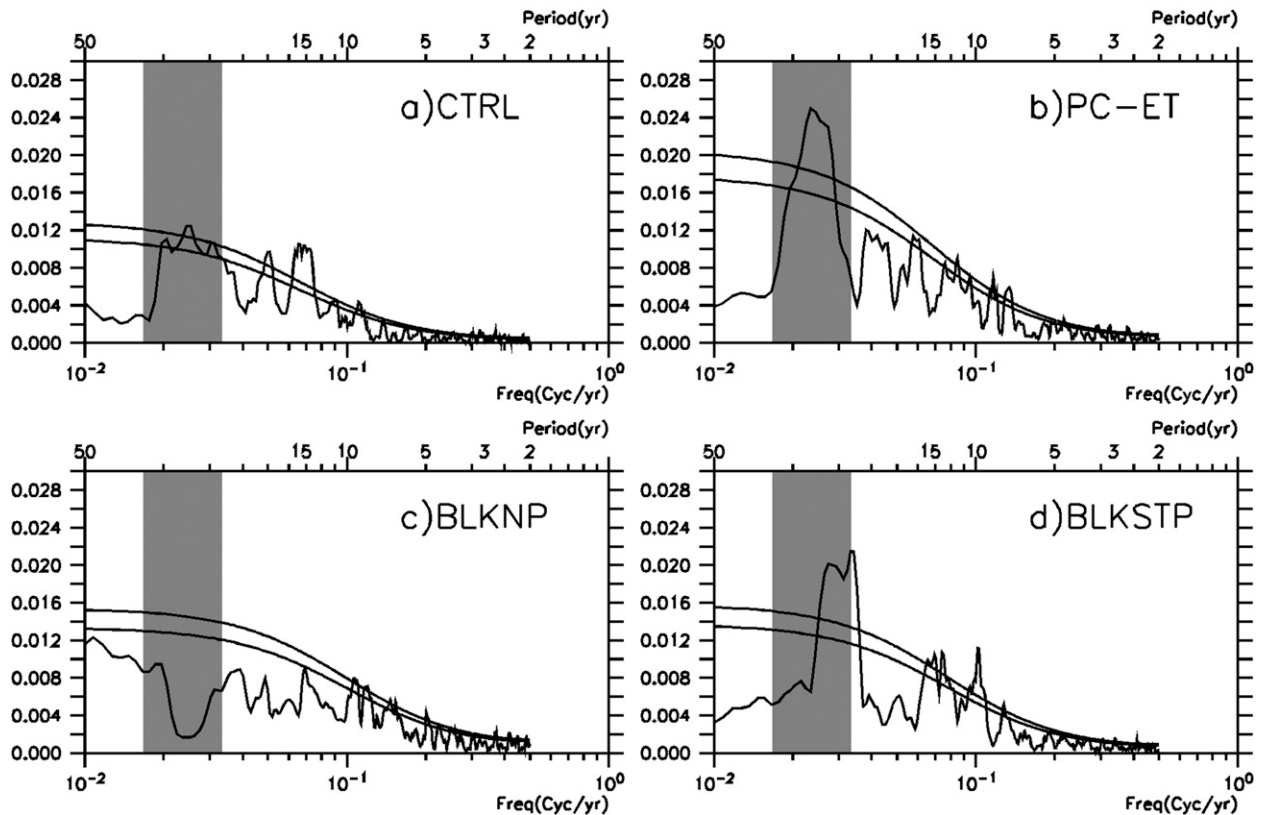
Power spectra

FIG. 2. Power spectra of unfiltered SST averaged over the west-central North Pacific in (a) CTRL, (b) PC-ET, (c) BLKNP, and (d) BLKSTP. The 95% and 90% confidence levels are indicated. The quasi-50-yr frequency band is highlighted with shading.

exhibiting the heaviest loading (over 0.3°C) along the KOE as well as substantial variability in the western subpolar gyre. This suggests that the PMV is independent of tropical ocean–atmosphere coupled variability. To further understand the region where ocean dynamics are crucial for PMV in PC-ET, we now focus on the two PB experiments in which Rossby wave propagation is blocked from crossing the midbasin. When Rossby waves are blocked in the subtropics (BLKSTP, Fig. 1d), the PMV SST variance remains similar to that in CTRL and PC-ET. This suggests that Rossby wave propagation in the subtropics is not critical for PMV. However, when Rossby wave propagation is blocked beyond the subtropics, all the way in the North Pacific (BLKNP, Fig. 1c), the PMV SST variance is reduced significantly. The maximum loading in the KOE is now reduced by ~50% to below 0.2°C. Most strikingly, the activity center in the subpolar North Pacific is suppressed almost completely. Together, the two experiments demonstrate explicitly that the Rossby wave propagation in the mid-to-high latitudes is critical for the PMV. In the meantime, the leading EOF of the multidecadal SSTs resembles the

classical horseshoe-like structure (Mantua et al. 1997) for all the cases (not shown). This suggests that the pattern of the PMV is set up predominantly by local atmospheric variability forcing.

We further examine the PMV by studying the power spectrum for unfiltered SST anomalies averaged over the center of PMV SST variability in the broad KOE region (35°–45°N, 140°E–140°W; denoted by the rectangular box in Fig. 1a). The distinguished PMV peaks at quasi-50-yr in CTRL (Fig. 2a) and PC-ET (Fig. 2b; Zhong et al. 2008). This peak is largely reproduced in BLKSTP (Fig. 2d) but is suppressed almost completely in BLKNP (Fig. 2c). The same conclusion can be drawn using other SST indices, including the leading principle component of the unfiltered SSTs in the North Pacific that corresponds to the horseshoe-like mode. The power spectral analysis (Fig. 2) therefore yields the same conclusion as that from the SST variance in Fig. 1: the PMV is suppressed in BLKNP but unchanged in BLKSTP. Thus, the wave propagation in mid-to-high latitudes of the North Pacific is crucial to the generation of the PMV, whereas that in the subtropical latitudes is not.

4. Life cycle of PMV: Evolution of ocean temperature and salinity anomalies

Further insight into the physical mechanism of the PMV can be gained by a comprehensive analysis of the PMV in PC-ET, including the life cycle, heat and salt budget, and other relevant physical processes. Because of the dominant contribution of salinity to the density gradient in the subpolar gyre (Cooper 1988), the role of salinity is given special attention. In our analysis below, special attention will be paid to positive feedbacks and delayed negative feedbacks. These two elements are critical to a general oscillatory variability mode, either a self-excited unstable mode or a noise-driven damped mode. Positive feedbacks are essential during the growth stage of the anomaly, whereas the delayed negative feedback is critical for the time-scale selection of the variability and its phase transition.

The evolution of the multidecadal temperature and salinity anomalies associated with the PMV can be shown as the lagged regression map of SST and sea surface salinity (SSS) upon a PMV index, which is chosen as the SST in the KOE region (35°–45°N, 140°–170°E; Fig. 3). Here, we only present the PMV analysis in PC-ET, whereas similar results are obtained for the PMV in CTRL and BLKSTP. To focus on the multidecadal variability, all data will be first bandpass filtered in the 25–80-yr band before regression. At a lag of −16 yr (Fig. 3, top), the PMV is nearly in its mature cold phase, characterized by dominant cold fresh surface water in the midlatitude North Pacific around the KOE region as well as modest warm saline water in the subpolar region. The cold/freshwater in the midlatitude then decays while the warm saline subpolar anomaly grows (lag of −12 yr; Fig. 3, second row). Later, the warm saline subpolar surface water extends into the midlatitude KOE region at a lag of −8 yr (Fig. 3, third row), switching the sign of the PMV. This warm saline anomaly in the KOE region then amplifies, peaking at a lag of 0 yr (Fig. 3, fourth and fifth rows). In the subpolar region, the cold fresh anomaly emerges from the eastern side, before the 0-yr lag, and subsequently grows and expands westward, completing half of the cycle.

The life cycle suggests some lead–lag relations. One feature is a clear lead of the surface anomaly in the subpolar region to that in the midlatitude KOE region. This lead–lag relation is better illustrated in the vertical transect along a track in the western Pacific from the subpolar region to the subtropics (marked in Fig. 3b, third row) in Fig. 4. Note that the mean boundary current flows largely along the transect at the subpolar latitudes. From a lag of −16 yr (Fig. 4, top), the warm saline anomaly in the subpolar region appears to be advected southward by the Oyashio in the surface 200 m (winter mixed layer), leading to the demise of the cold fresh anomaly in the KOE (Fig. 4, second row) and the subsequent emergence of the warm saline condition at a lag of −8 yr (Fig. 4, third row). The warm saline anomaly in KOE then intensifies and expands with depth, peaking at a lag of 0 yr (Fig. 4, fifth row). The evolution in Fig. 4 also suggests a lead of the subsurface anomaly to the surface anomaly in the subpolar region. It is seen that a cold anomaly forms in the subsurface of the subpolar region at a lag of −12 yr (Fig. 4a, second row) and maximizes later at a lag of 0 yr. The cold anomaly appears to be upwelled, eventually reversing the warm saline surface water into cold fresh water at a lag of 4 yr (Fig. 4, sixth row). Together, the multidecadal signal appears to emerge first in the subsurface subpolar gyre, then ascends to the surface, and eventually travels southward to the KOE region.

The life cycle study above identified three key regions for PMV: the subsurface western subpolar Pacific, the surface western subpolar Pacific, and the KOE. The relative phasing among these key regions is seen more clearly in their lead–lag correlation with the KOE SST in Fig. 5 for both the temperature and salinity variability. The temperature (Fig. 5a) and salinity (Fig. 5b) signals tend to vary in phase in the surface. This surface temperature–salinity compensation on the halocline background stratification suggests the role of local convective instability—a point to return to later. It is seen that the subsurface subpolar anomaly leads the surface subpolar anomaly by a quarter of cycle (i.e., ~10 yr), and the latter leads the KOE anomaly by another quarter of cycle. Thus the KOE appears to be out of phase with the subsurface subpolar anomaly. This raises the following question: what is the physical mechanism for such a phase relationship?

5. Physical processes driving the life cycle of PMV

Here we examine in detail the physical linkages (i) from the KOE to the subsurface subpolar region, (ii) from the subsurface to the surface subpolar region, and (iii) from the surface subpolar region to the KOE.

a. From the KOE to the subsurface subpolar region: Phase reversal and initial growth

The connection from the KOE to the subsurface subpolar ocean depends critically on the atmospheric bridge. A warm anomaly in the KOE tends to produce an anomalous anticyclonic wind curl and in turn downward Ekman pumping over the subpolar Pacific Ocean (Fig. 6a). The persistent wind curl and downward Ekman pumping response to the long-term PMV oceanic anomaly
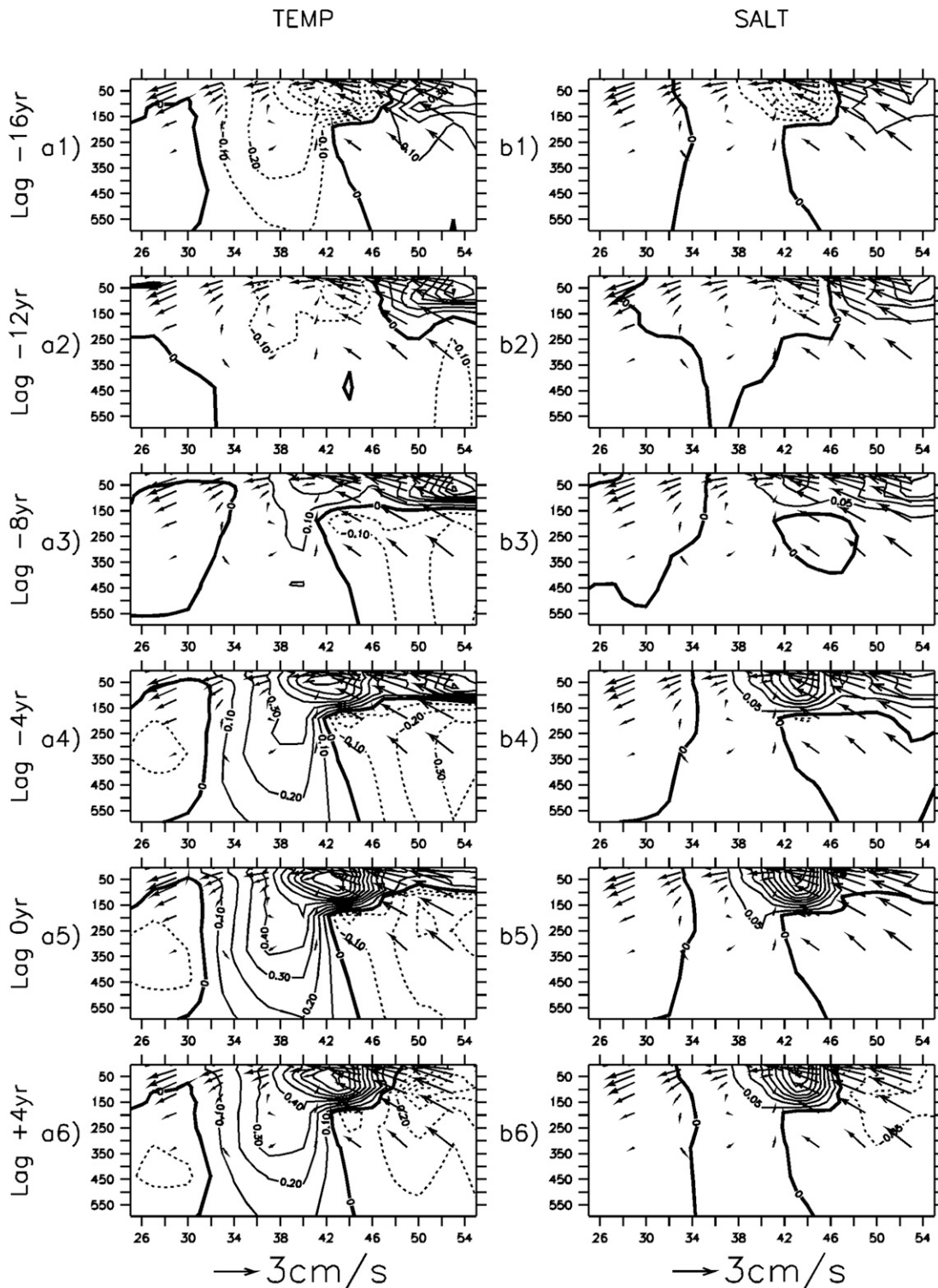
SST

SSS

FIG. 3. Lagged regression of (a) SST and (b) SSS on the normalized SST time series in the KOE (35°–45°N, 140°–170°E). All data are 25–80-yr band filtered before regression. Negative (positive) lags indicate KOE SST lagging (leading). Lags are for the following: (top)–(bottom) −16, −12, −8, −4, 0, and +4 yr. CI = 0.1°C °C^{-1} and 0.05 psu °C^{-1} for SST and SSS, respectively. (b3) The starred track line represents the section on which Fig. 4 is based.

TEMP   SALT

FIG. 4. Lagged regression of (a) temperature and (b) salinity upon the normalized SST in the KOE. The vertical section is along the track line in Fig. 3. All data are 25–80-yr band filtered before regression. Lags are for the following: (top)–(bottom) −16, −12, −8, −4, 0, and +4 yr. CI = 0.1°C °C^{-1} and 0.05 psu °C^{-1} for temperature and salinity, respectively. Also shown in vector is the mean climatology of meridional and vertical current with the latter multiplied by 1×10^4. Unit length of vector represents 3 cm s^{-1}.
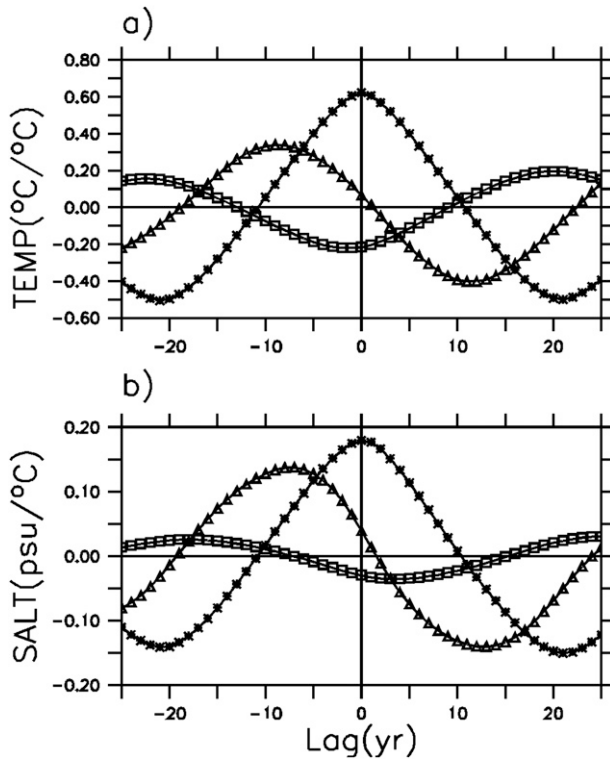
FIG. 5. Lagged regression of (a) temperature and (b) salinity in the surface of the subpolar region (triangles; 48°–55°N, 160°E–180°, 0–100 m), subsurface of the subpolar region (squares; 48°–55°N, 160°E–180°, 170–370 m), and surface of the KOE (stars; 35°–45°N, 140°–170°E, 0–50 m) upon the normalized SST in the KOE. All data are 25–80-yr band filtered before regression.
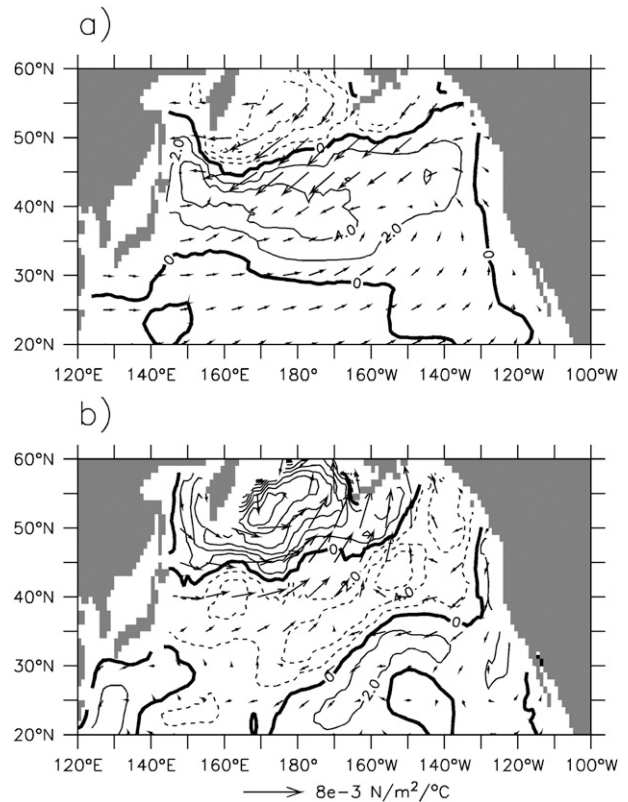

FIG. 6. Lagged regression of wind curl (contour) and wind stress (vector) on the normalized SST in the KOE. The atmosphere (a) lagging SST by 1 yr and (b) leading SST by 10 yr; all variables are 25–80-yr band filtered before regression. Unit length of vector represents 8×10^{-3} N m^{-2} °C^{-1}. CI = 2×10^{-9} N m^{-3} °C^{-1} for wind curl.

(Liu et al. 2007; Zhong and Liu 2008) would then depress the thermocline or halocline and increase the ocean dynamic height. The thermocline or halocline anomaly then propagates westward across the basin via planetary waves (Schneider et al. 2002). This wind-forced response can be seen in the evolution of dynamic height at 250-m depth in Fig. 7. In response to a cold anomaly in the KOE, an anomalous cyclonic wind curl forcing and resultant Ekman suction generate a negative dynamic height anomaly in the eastern basin of the subpolar Pacific and its subsequent westward propagation with intensification (Fig. 7a, first–fourth rows).

How is the dynamic height anomaly linked to the temperature and salinity anomalies of interest, then? We resort to the two classical perspectives on ocean dynamic height (Landerer et al. 2007). From the steric perspective, dynamic height anomaly can equivalently be interpreted in terms of the integral response to anomaly in the vertical density distribution through temperature and salinity anomaly. A breakdown of the dynamic height into temperature- and salinity-related components (Fig. 8) manifests the predominance by the salinity-

related component, as previously discussed. In the subpolar North Pacific (e.g., 50°N), the salinity-related component largely resembles the total dynamic height (in particular, to the east of 180°) and exhibits clear westward propagating signal (Fig. 8a). The salinity anomaly herein is created by uplift of the halocline associated with the wave propagation. More specifically, an uplift of halocline brings salty water upward, producing a salty dense anomaly and thus a negative dynamic height anomaly. The temperature-related component differs substantially, with little signal of sustainable westward propagation (Fig. 8b). This is because processes (e.g., horizontal advection) other than the vertical undulation of thermocline determine the temperature anomaly, as will be demonstrated later.

From the dynamic perspective, a current anomaly, in geostrophic balance with gradient of the dynamic height anomaly, may alter the temperature and salinity distribution. As the wave propagates into the western subpolar Pacific, the negative dynamic height anomaly (Fig. 7a, fourth row) builds up a northeastward current anomaly to
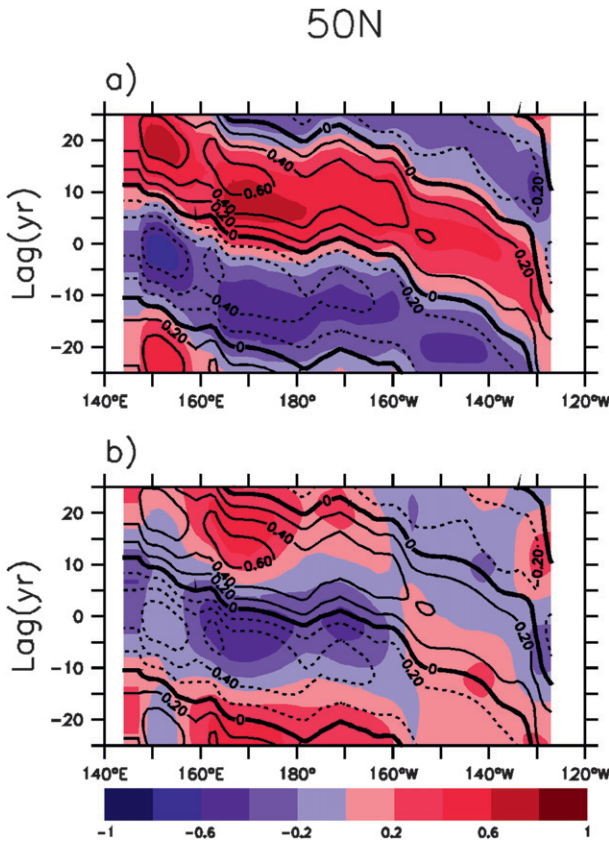
FIG. 7. Lagged regression of (a) ocean dynamic height (shading) and Ekman pumping (contour), (b) geostrophic current (flowline), (c) temperature, and (d) salinity at 250-m depth on the normalized SST in the KOE. All data are 25–80-yr band filtered before regression. Lags are for the following: (top)–(bottom) −20, −16, −12, −8, −4, 0, and +4 yr. CI = 3×10^{-6} cm $°C^{-1}$, 0.3 m $°C^{-1}$, 0.1°C, 0.05 psu $°C^{-1}$ for Ekman pumping (downward in negative value), ocean dynamic height, temperature, and salinity, respectively. The size of the arrows in (b) indicates the speed of the flow. Mean climatology of ocean temperature at 250 m is also shown in (b) in color, with the rectangular box delineating the subpolar North Pacific (48°–55°N, 160°E–180°W).

50N

FIG. 8. Lagged correlation of the (a) salinity- and (b) temperature-related components of the dynamic height (shading) and total dynamic height averaged in the upper 500 m (contour) upon the normalized SST in the KOE. All data are 25–80-yr band filtered before regression.

its southeast (Fig. 7b, fourth row), which begins to prevail in the western subpolar Pacific (denoted by the rectangular box in Fig. 7) and leads to cooling (Fig. 7c, fourth row) and freshening in the subsurface (Fig. 7d, fourth row) resulting from attenuation of the warm salty flow from the east. It is this anomalous horizontal heat advection that determines the temperature variability. The cooling effect of anomalous horizontal heat advection reverses the temperature variability into its cold phase and then solidifies it further on. The freshening effect of this anomalous horizontal advection also assists the phase transition of salinity variability in the western subpolar Pacific (Fig. 7d, fourth row). In some sense, the salinity variability appears to contain a self-oscillatory seed pertaining to the intimately linked "steric" and "dynamic" ocean dynamic height. In short, via large-scale air–sea interaction, a cold fresh anomaly in the KOE tends to create a cold fresh anomaly in the subsurface of the western subpolar Pacific in about 20 yr (i.e., half of a period of the multidecadal cycle).

b. From the subsurface to the surface subpolar region: Transmission and amplification

In the subpolar Pacific Ocean, a robust route for the subsurface temperature salinity anomalies to influence the surface is the mean upwelling current forced by the prevailing cyclonic wind curl. As seen in the life cycle in Fig. 4, a cold fresh anomaly originated in the subsurface upwells to the surface, diminishing the warm salty anomaly at the surface (Fig. 4, fourth and fifth rows) and later fostering a cold fresh anomaly there (Fig. 4, sixth row). The cold fresh anomaly at the surface then grows via positive feedbacks that hinge on the mean stratification of the subpolar Pacific, as discussed later (Fig. 4a, first and second rows).

A characteristic feature of the mean stratification in the northern subpolar North Pacific is a dominant halocline with a strong freshening from 600-m depth upward to the surface mixed layer (Fig. 9b). The surface freshening is caused by the ample precipitation associated with the storm track, which overwhelms the evaporative contribution to salinity, the latter being small for the near-freezing surface temperature in the northern subpolar North Pacific. Accompanied with this halocline is a mean temperature inversion, with the temperature decreasing upward from about ~400-m depth toward the surface (Fig. 9a), where it is cooled by strong heat loss associated with turbulent heat flux and net radiative cooling. Similar to the long-term climatology of stratification there, the density variability of the PMV in the subpolar upper ocean is also dominated by the salinity contribution, as indicated in the T–S diagram in Fig. 9c. Surface cooling and freshening lead to a density reduction because of the strong negative damping of the surface temperature anomaly resulting from the turbulent heat fluxes. The reduced density in turn leads to a shallower mixed layer (Fig. 9d), which then leads to less warm salty water being entrained from the subsurface into the mixed layer, further amplifying the initial surface cooling freshening. This convective instability, which has been studied by Lenderink and Haarsma (1994), provides a positive feedback that helps to amplify a PMV anomaly here. This positive feedback was also found to be important for decadal variability of the thermohaline circulation in ocean model simulations using a mixed boundary condition (restoring on temperature and fixed flux for salinity; Arzel et al. 2006).

The subpolar PMV anomaly may also be amplified by another positive feedback associated with local air–sea interaction. A surface cold anomaly tends to induce an atmospheric response with a local anticyclonic wind curl anomaly (Zhong and Liu 2008), which generates a downward Ekman pumping anomaly that reduces the
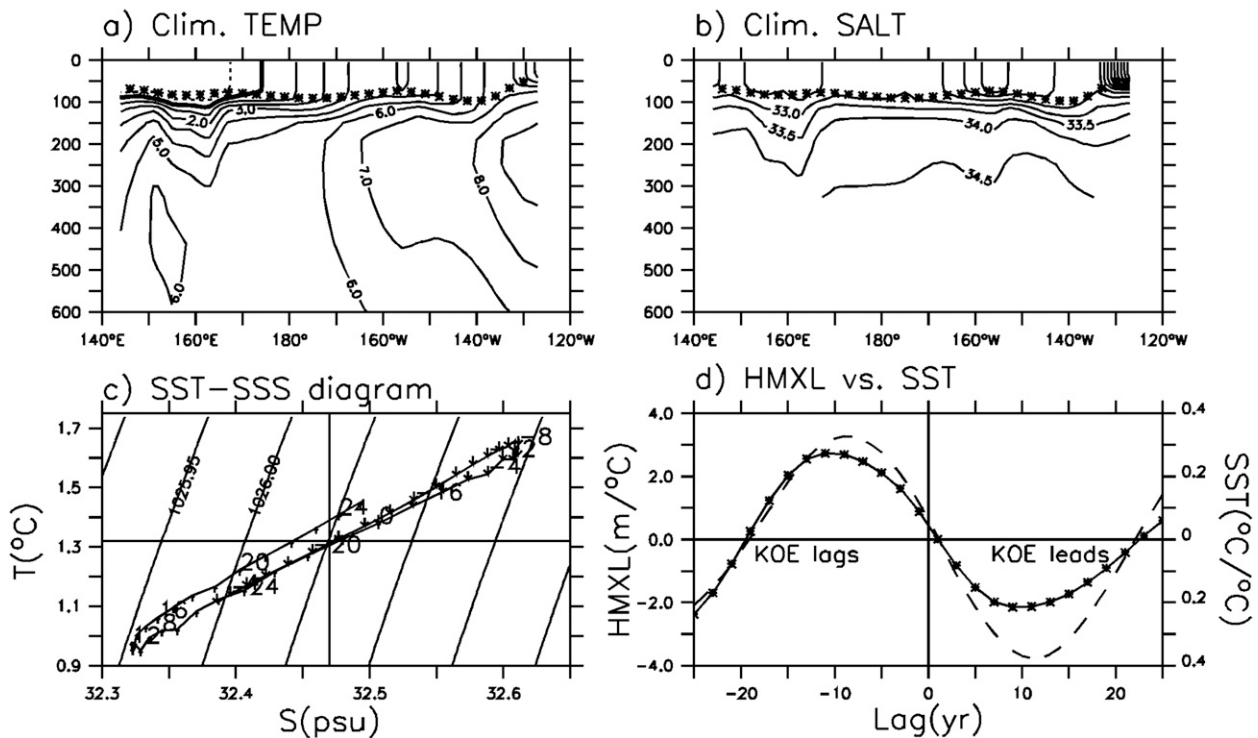
Subpolar

FIG. 9. (a) Mean climatology of ocean temperature in wintertime (December–February) at 50°N. CI = 1°C. Mean mixed layer depth in wintertime is delineated with steroid. (b) Mean climatology of ocean salinity in wintertime at 50°N. CI = 0.5 psu. (c) SST–SSS plot of the multidecadal cycle for the subpolar region (48°–55°N, 160°E–180°) with corresponding tilting density contours (kg m^{-3}). The arrows connected by the black line represent the variability in SST–SSS through the multidecadal cycle, with downward (upward) arrows at negative (positive) lags. The corresponding lag is labeled for every 4 yr. The SST and SSS variability is obtained by regression on the normalized SST in the KOE. (d) Lagged regression of mixed layer depth in wintertime (steroid) and SST (dashed) at 53°N, 170°E on the normalized SST in the KOE. All data are 25–80-yr band filtered before regression.

upwelling of warm salty water into the surface mixed layer; it also intensifies the surface temperature and salinity anomalies.

c. From the surface subpolar region to the KOE: Transmission and amplification

After emerging from the subsurface to the surface in the western subpolar North Pacific, the PMV signal appears to be advected to the KOE region along the southward Oyashio (Fig. 4). Upon reaching the northern part of the KOE, the signal is further amplified through a similar convective positive feedback. As a warm saline anomaly arrives at the northern part of the KOE (42°–46°N, 148°–170°E; Fig. 4, third row), the surface density is increased (Fig. 10c), which deepens the mixed layer (Fig. 10d) and induces more warm salty subsurface water being entrained to the surface, further amplifying the initial warm salty anomaly. Thereafter, the convective feedback keeps the multidecadal anomaly growing (Fig. 4, fourth and fifth rows).

The PMV anomaly could also be reinforced by another positive feedback associated with surface wind. A warm anomaly in the KOE favors a downstream low pressure response in CCSM3 (and vice versa; Zhong and Liu 2008). The associated response in the wind stress field exhibits an easterly anomaly over the west-central North Pacific (Fig. 6a), which would generate an anomalous northward Ekman transport in the surface ocean and further increase the warm salty anomaly.

The physical processes involved in a life cycle of PMV are illustrated with the schematic diagram in Fig. 11. Starting from a mature cold phase of the PMV (Fig. 11a), the KOE exhibits maximum cooling, whereas the subsurface subpolar ocean shows a significant warming. The latter upwells to the surface and grows via positive feedbacks associated with convection and Ekman pumping (Fig. 11b). The warm saline surface anomaly is then advected southward along the Oyashio. Upon reaching the KOE, the warm anomaly is further amplified through the convective feedback and wind-related feedback and
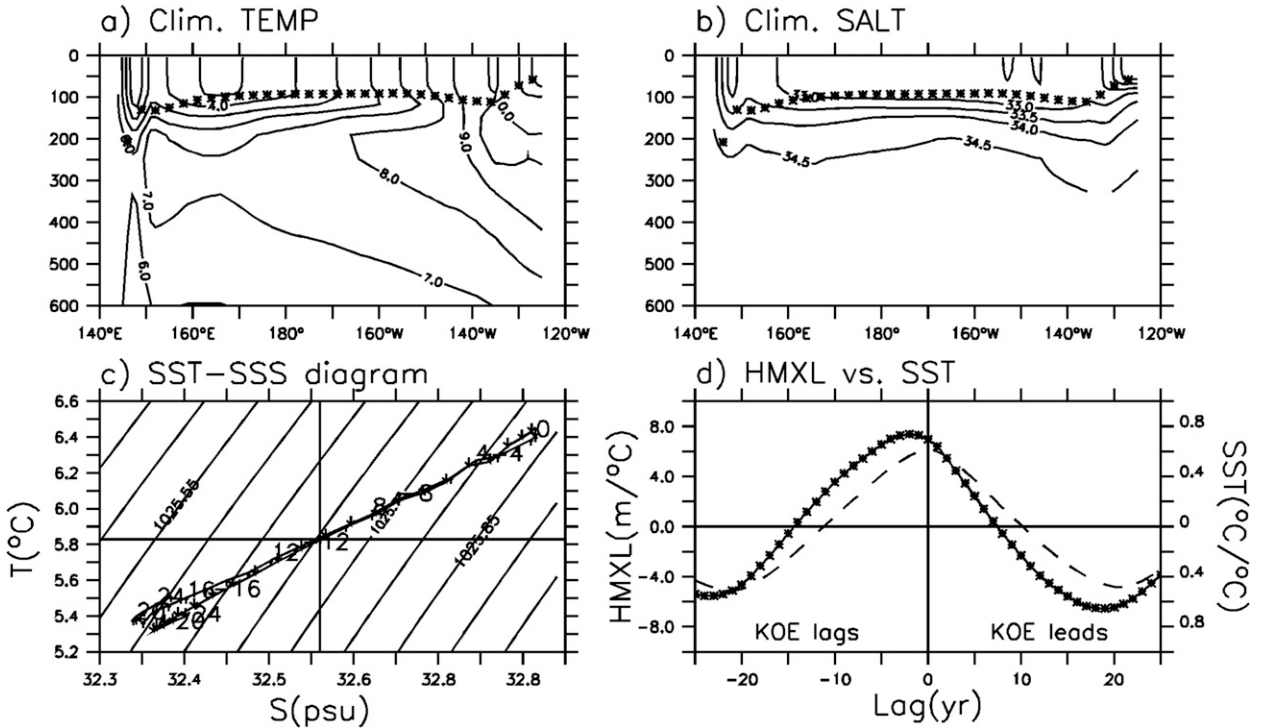
N. KOE

FIG. 10. As in Fig. 9, but for (a),(b) 44°N; (c) the northern KOE (42°–46°N, 148°–170°E); and (d) 44°N, 152°E.

finally peaks at a lag of 0 yr (Fig. 11c). In the meantime, the original cold anomaly in the KOE (Fig. 11a) induces an anomalous cyclonic wind curl over the subpolar region, which would generate a propagating dynamic height anomaly and hence create a cold fresh anomaly in the subsurface of the subpolar region in 20 yr or so (Fig. 11c). Thereby, the mature warm phase of the PMV is established and starts to evolve into the other half of the cycle.

6. Heat and salt budget analyses

The mechanism of the PMV studied above is now further substantiated with heat and salt budget analyses. The heat and salt budgets are reconstructed offline using the monthly output, according to the formulas

$$d(T + t)/dt = \underset{(i)}{\text{SHF}} + \underset{(ii)}{(-\overline{U}T'_x - \overline{V}T'_y - \overline{W}T'_z)}$$
$$+ \underset{(iii)}{(-u'\overline{T}_x - v'\overline{T}_y - w'\overline{T}_z)} + \underset{(iv)}{\text{T\_RES}} \quad \text{and}$$

(1a)

$$d(S + s)/dt = \underset{(i)}{\text{SFLX}} + \underset{(ii)}{(-\overline{U}S'_x - \overline{V}S'_y - \overline{W}S'_z)}$$
$$+ \underset{(iii)}{(-u'\overline{S}_x - v'\overline{S}_y - w'\overline{S}_z)} + \underset{(iv)}{\text{S\_RES}}, \quad (1b)$$

where T is the temperature, S the salinity, U the zonal velocity, V the meridional velocity, and W the vertical velocity. Time mean field is denoted in uppercase, anomaly field in lowercase, and differential field with subscript. The major terms to be calculated on the right-hand side of Eqs. (1a) and (1b) are the following: (i) the local temperature or salinity change, surface heat flux (SHF) or surface salt flux (SFLX); (ii) the mean advection across the anomalous temperature or salinity gradient and (iii) anomalous advection across the mean temperature or salinity gradient in both horizontal and vertical directions; and (iv) the temperature (T_RES) or salt residual (S_RES), which includes all the remaining terms such as mixing and diffusion.

a. The subsurface subpolar region

The evolution of dominant heat and salt budget terms in the subsurface subpolar ocean is shown in Figs. 12a,b as the lagged regression on the KOE SST after a 25–80-yr bandpass filtering. To better illustrate positive and negative feedbacks, the change rate of temperature or salinity variance resulting from each term is also calculated (Figs. 12c,d) following Solomon et al. (2003), where a positive (negative) term is responsible for the instantaneous growth (decay) of the magnitude of the
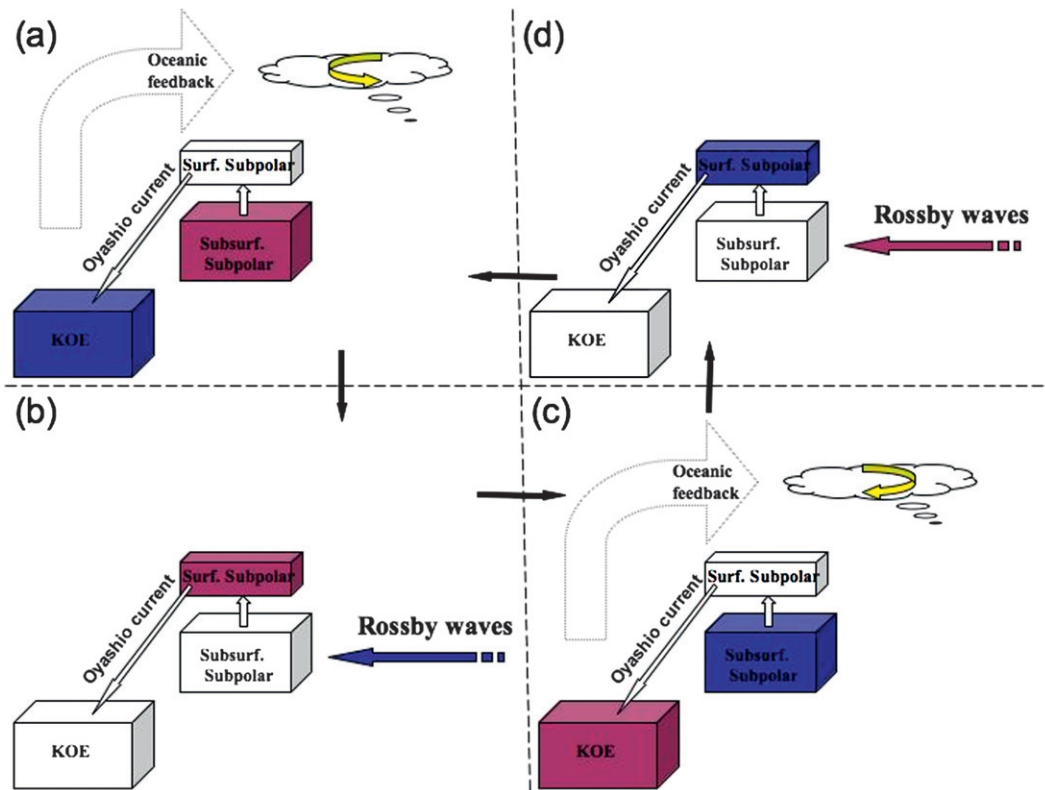
FIG. 11. Schematic picture of a full cycle of PMV. Explanation is given in the text.

anomaly, regardless of its sign. The heat budget shows that during most of the PMV cycle the anomalous horizontal advection across mean gradient provides the growth mechanism, whereas the mean advection across anomalous temperature gradient acts to dissipate the anomaly, which is in agreement with the physical description in section 5a (see discussion on Fig. 7). The anomalous advection across mean horizontal gradient associated with Rossby wave propagation gives rise to the temperature anomaly. Once a temperature anomaly is generated in the subsurface, it is advected away by the mean upward current.

This anomalous advection functions similarly in the salt budget, providing phase switching and initial growth mechanisms, as evident by its leading (∼4 yr) the salinity anomaly (Fig. 12b). Further growth of the salinity anomaly is driven by the anomalous vertical advection across mean stratification, slightly lagging (∼4 yr) the salinity anomaly. Physically, the vertical undulation of halocline intensifies the foregoing salinity anomaly while the wave propagates into the western subpolar Pacific. Like the temperature anomaly, the salinity anomaly is also advected away by the mean upward current. It should be pointed out that from the equations for the temperature and salinity variance, this amplify-

ing mechanism resulting from the anomalous current also corresponds to a downgradient eddy-density flux [e.g., for temperature, $-(u^*t)T_x - (v^*t)T_y > 0$], which may also be related to the instability of planetary Rossby waves, which has been suggested to be important for the generation of decadal variability in constant flux-forced ocean models (Colin de Verdière and Huck 1999).

b. The surface subpolar region

The heat budget for the surface subpolar region is dominated by the surface heat flux, anomalous horizontal and vertical advection across the mean gradient, mean vertical advection across the anomalous gradient, and the residual (Fig. 13). The surface heat flux is almost out of phase with the SST anomaly over most of the PMV cycle, implying a damping effect on the PMV. This damping effect of heat flux is interesting because it seems to contradict the monthly SST variability in the extratropics that tends to be driven by the heat flux in the observation (Frankignoul et al. 1998). A closer examination reveals a strong time-scale dependence of the effect of surface heat flux on SST (Fig. 14). At a monthly time scale, the correlation between heat flux and SST is characterized by a dual-peak structure: a positive peak at SST lagging heat flux by 1 month and a negative peak

SUBSFC SP
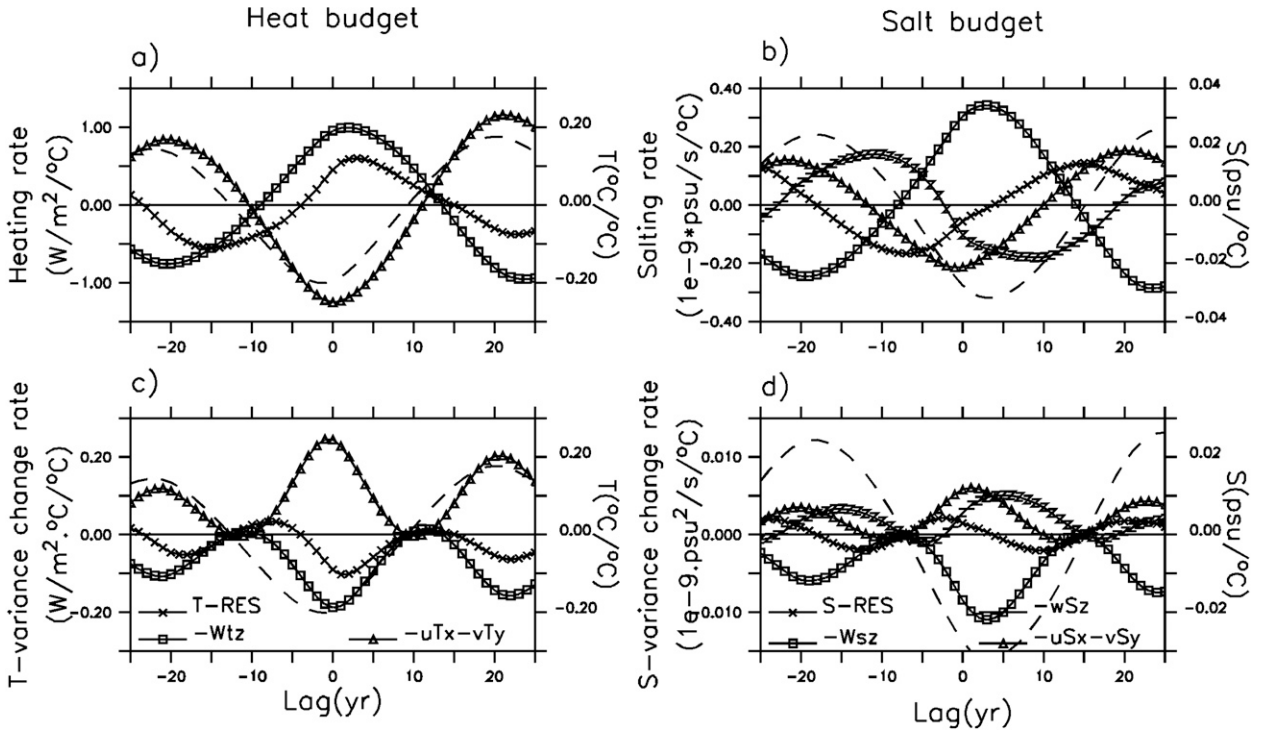
Heat budget

Salt budget

FIG. 12. Lagged regression of dominant (a) heating and (b) salting terms and induced change rate in (c) temperature and (d) salinity variance averaged over the subsurface of the western subpolar North Pacific (48°–55°N, 160°E–180°W, 170–370 m) on the normalized SST in the KOE. Also shown in the dashed curve is the (a),(c) temperature and (b),(d) salinity in the subsurface of the subpolar North Pacific. The 25–80-yr band filter is applied before regression. The curves in (a) and (c) indicate mean vertical advection of temperature anomaly ($-Wt_z$; squares), anomalous horizontal advection across mean gradient ($-uT_x - vT_y$; triangles), and the residual (T_RES; crosses); (b) and (d) mean vertical advection of salinity anomaly ($-Ws_z$; squares), anomalous horizontal advection across mean gradient ($-uS_x - vS_y$; triangles), anomalous vertical advection across mean gradient ($-wS_z$; zs); and the residual (S_RES; crosses).

with the SST leading heat flux by 1 month (Fig. 14a). This dual-peak correlation structure is consistent with previous works (Frankignoul et al. 1998; Barsugli and Battisti 1998). Physically, it implies that a downward surface heat flux rapidly induces a warm SST anomaly (the positive peak with SST lagging), which is then damped by heat loss to the atmosphere (the negative peak with SST leading). The situation is the same for the interannual variability (Fig. 14b). In sharp contrast, however, at decadal (Fig. 14c) and multidecadal (Fig. 14d) scales, the peak correlation is found around a lag of 0. This suggests a primarily damping effect of surface heat fluxes on SST. Physically, this implies that a slow warm SST anomaly is generated by oceanic dynamic processes and is then damped by heat loss to the atmosphere (the potential impact of temporal smoothing on the correlation function is shown in the appendix for a conceptual stochastic climate model). Therefore, PMV differs fundamentally from short-term SST variability in the North Pacific; the latter is driven by the

atmosphere, whereas the former involves oceanic processes critically.

The growth of the multidecadal temperature anomaly in the subpolar surface is driven predominantly by the residual term, which is dominated by convection, as seen in the almost in-phase variation of the residual term with the SST (Fig. 13a) and the positive correlation with SST (Fig. 13c) over most of the PMV cycle. The phase-switching mechanism appears to be provided by the mean upward advection of the temperature anomaly as well as the anomalous horizontal advection across the mean gradient, as seen in a 90° phase lead of these two terms on SST in Fig. 13a. Consistent with our discussion in section 5b, this suggests that the mean upwelling current brings the subsurface temperature anomaly up to the surface and reverses the phase of the multidecadal variability. The anomalous horizontal advection also assists this transition as it does in the subsurface. Because of the halocline stratification there, the convection, mean upward advection, and anomalous horizontal
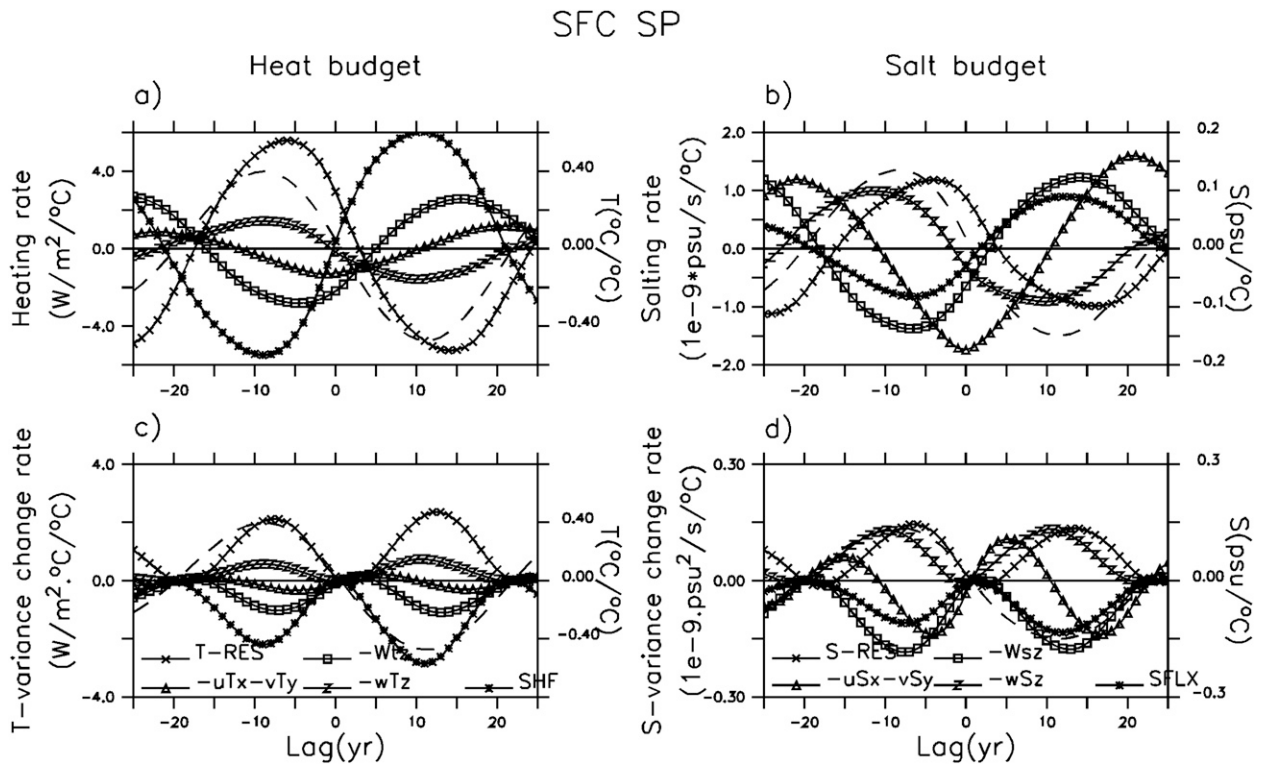
SFC SP

FIG. 13. As in Fig. 12, but for the surface of the western subpolar North Pacific (48°–55°N, 160°E–180°, 0–100 m). (a),(c) The curves indicate surface heat flux (SHF; stars), anomalous horizontal advection across mean gradient ($-uT_x - vT_y$; triangles), anomalous vertical advection across mean gradient ($-wT_z$; zs), mean vertical advection of temperature anomaly ($-Wt_z$; squares), and the residual (T_RES; crosses). (b),(d) The curves indicate surface salt flux (SFLX; stars), anomalous horizontal advection across mean gradient ($-uS_x - vS_y$; triangles), anomalous vertical advection across mean gradient ($-wS_z$; zs), mean vertical advection of salinity anomaly ($-WS_z$; squares), and the residual (S_RES; crosses).

advection across the mean gradient all play a similar role in the salt budget, helping to build an SSS anomaly in the surface (Figs. 13b,d). Once the SST or SSS variability is phase-reversed by the mean upwelling, the resultant anomaly in surface density and convection provides the growth mechanism for the multidecadal anomaly in the surface of western subpolar Pacific. Besides, the oceanic anomaly would induce a local wind curl anomaly, which in turn forces anomalous Ekman pumping and further amplifies the SST or SSS anomaly.

c. The northern KOE

As for the surface subpolar region, the convection is a major growth mechanism in both the heat and salt budget, which is inferable from its largely in-phase relation with the SST and SSS (Figs. 15a,c) and the overall positive correlation (Figs. 15b,d). The anomalous convection is triggered by the southward mean advection of the multidecadal anomaly from the subpolar region. As discussed in section 5c, the SST or SSS anomaly, which is transmitted from the western subpolar Pacific, would

alter the stratification and thus incite anomalous convection. Integrated over the multidecadal cycle, anomalous horizontal advection across the mean gradient contributes positively to the SST or SSS variability, whereas mean horizontal advection carries the anomaly away and provides the decay (Figs. 15b,d). The former is attributable to the anomaly in Oyashio in association with the wave adjustment in the subpolar North Pacific. Notably, all these terms act the same way for both the SST and SSS anomalies. Distinctively, the surface flux plays an opposing role for the heat and salt budgets. The surface heat flux acts as a damping factor as indicated by its out-of-phase relation with temperature anomaly (Fig. 15a) and negative correlation (Fig. 15c), whereas the surface salt flux supplies an extra source for the salinity anomaly (Fig. 15d). A further decomposition suggests that the surface salt flux is led by the contribution from the melting anomaly (not shown). In the presence of a warm salty anomaly, the sea ice shrinks and less sea ice is subject to melting; as a consequence, less melting occurs, which reinforces the salty anomaly.
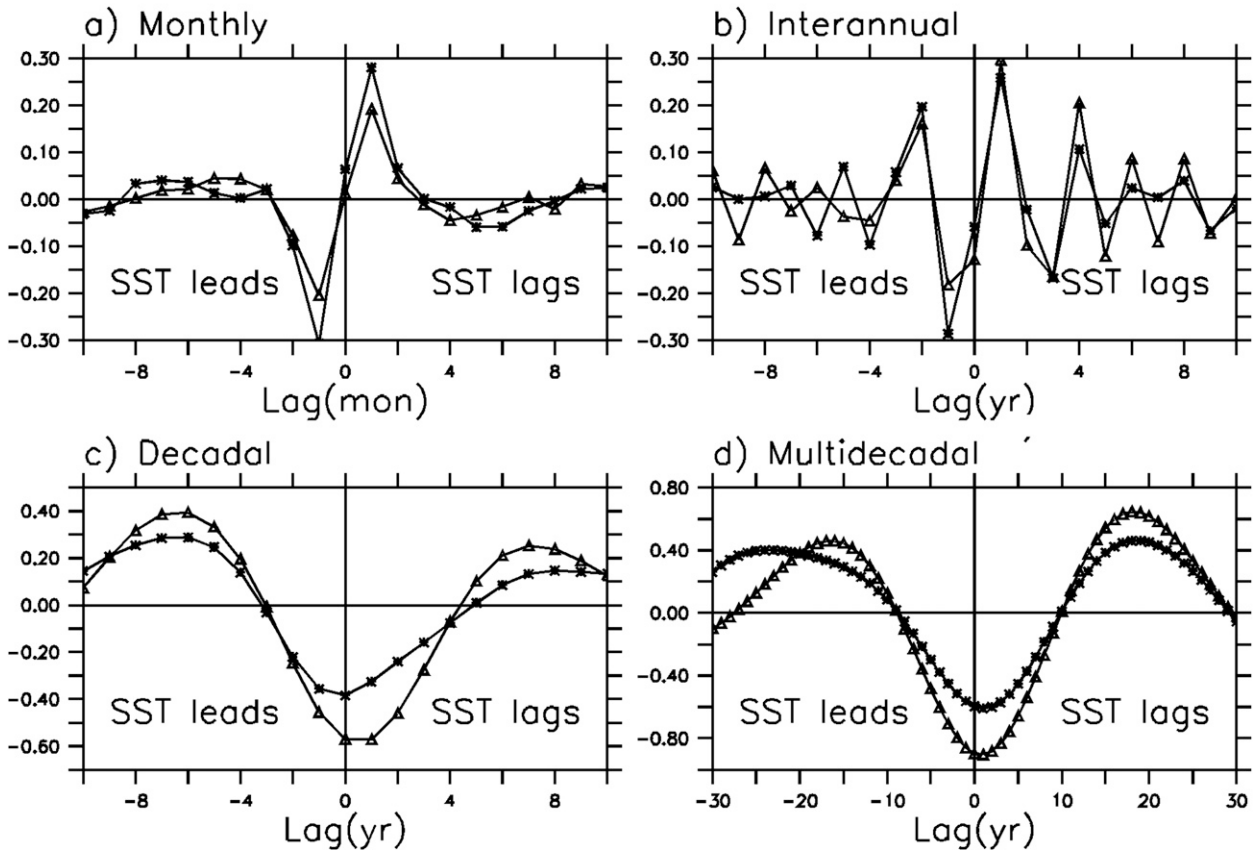
Lagged CORR(HFLX,SST)

FIG. 14. Lagged correlation of surface heat flux and SST in the subpolar region (triangles; 48°–55°N, 160°E–180°) and KOE (stars; 35°–45°N, 140°–170°E) at (a) monthly, (b) 1–5-yr, (c) 7–25-yr, and (d) 25–80-yr time scales. Monthly data are used for (a), whereas band-filtered annual data are used for (b)–(d).

Also of interest is the interrelationship of SST and SSS via precipitation and evaporation. A warm (cold) SST anomaly tends to induce stronger (weaker) evaporation and increased (decreased) precipitation, which results in a freshwater loss (gain) for the surface ocean and hence a salty (fresh) anomaly (not shown). The SST-induced variation in precipitation–evaporation thus acts as a positive feedback to the SSS variability in the KOE. It has been termed as the SST–evaporation–SSS mechanism and is speculated to be effective particularly at decadal and longer time scales (Frankignoul et al. 1998).

Overall, the physical description of PMV life cycle in section 5 is substantiated from both temperature and salinity standpoints.

7. Discussion and conclusions

Our analysis suggests that the temperature–salinity anomaly may originate from the subsurface subpolar region as a result of the planetary wave adjustment to the basin-wide wind curl forcing. This implies that the long-term memory of the PMV resides in the subsurface ocean. More specifically, the PMV time-scale selection seems to be associated with the first baroclinic-mode Rossby waves in the subpolar North Pacific. To observe the propagation of Rossby waves in a conventional way, we calculated the autocorrelation function (ACF) of monthly sea surface height (SSH) anomalies using a base point of 180°E. Following Jacobs and Mitchell (1996), the cross-basin zonal average is deducted before the ACF calculation to remove the steric effect. At 50°N, for example, there is a clear indication of westward propagating Rossby waves (Fig. 16). It takes about 25 yr to cross the Pacific basin, which appears to be relevant to the PMV time scale.

The speed of westward Rossby wave propagation in the North Pacific is further quantified both empirically and theoretically (Fig. 17). The empirical estimation
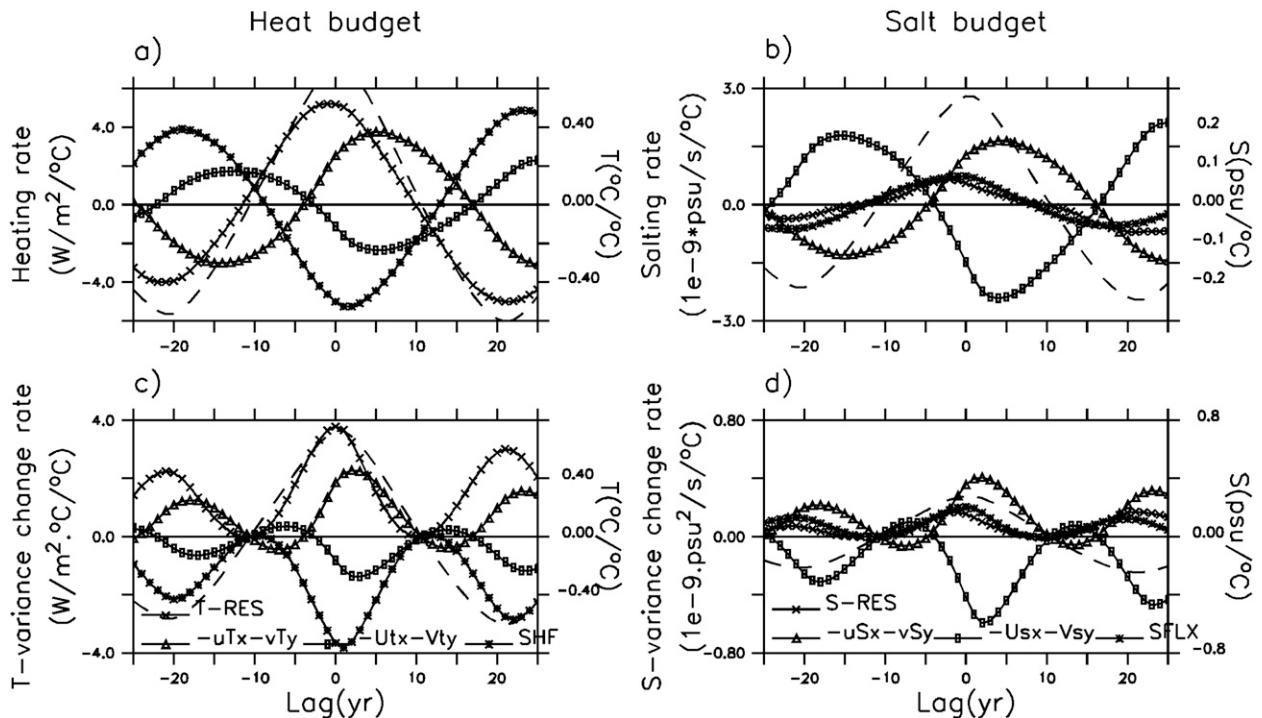
N. KOE

Heat budget

a)

Salt budget

b)

FIG. 15. As in Fig. 12, but for the surface of northern KOE (42°–46°N, 148°–170°E, 0–100 m). (a),(c) The curves indicate surface heat flux (SHF; stars), anomalous horizontal advection across mean gradient ($-uT_x - vT_y$; triangles), mean horizontal advection of temperature anomaly ($-Ut_x - Vt_y$; rectangles), and the residual (T_RES; crosses). (b),(d) The curves indicate surface salt flux (SFLX; stars), anomalous horizontal advection across mean gradient ($-uS_x - vS_y$; triangles), mean horizontal advection of salinity anomaly ($-Us_x - Vs_y$; rectangles), and the residual (S_RES; crosses).

uses the two-dimensional (longitude–time) spectrum, as in Jacobs and Mitchell (1996), whereas theoretical calculation solves the eigenvalue problem based on the mean model ocean stratification, following the approach of Chelton et al. (1998) and Chelton and Schlax (1996). The empirically estimated wave speed is largely consistent with that from the observation and tends to be faster than the theoretical speeds (Chelton and Schlax 1996; Qiu 2003; Kwon and Deser 2007). At 50°N, the estimated speed is 0.87 cm s^{-1}, equivalent to a cross-basin time scale of ~25 yr, which is consistent with Fig. 8. The evidence that the propagation is related to the first baroclinic-mode Rossby waves also comes from that fact that the propagation signal is dominant in the surface dynamic height field—a characteristic of the first baroclinic mode (Liu 1999a,b).

It is also interesting to discuss the dissipation rate of the subpolar Rossby waves. Dissipation rate is important because it impacts the significance of Rossby wave propagation in low-frequency variability. A weaker dissipation rate makes the wave propagation more important because the waves are allowed to propagate over a longer time

scale (Schneider et al. 2002; Kwon and Deser 2007). As discussed before in section 5a, the density anomaly associated with the PMV in the subpolar North Pacific is dominated by the contribution from the salinity anomaly. Unlike an SST anomaly that is subject to strong negative feedback with the atmosphere and therefore damps quickly (Frankignoul et al. 1998), an SSS anomaly in the mixed layer can persist at a longer time scale (indeed, in the subpolar region, the decorrelation time is 2 and 3 yr for SST and SSS, respectively). This suggests that Rossby wave propagation in the subpolar North Pacific is likely subject to less dissipation relative to that in the lower latitude, say, in the subtropics. In the subtropics, the density anomaly is dominated by temperature, which can be damped severely at the surface because of the air–sea interaction.

The key role of salinity is also appreciable in the convective growth mechanism as well. Through its predominant contribution to surface density variability, the salinity variability modifies the stratification and thus the convective activity in the western subpolar region
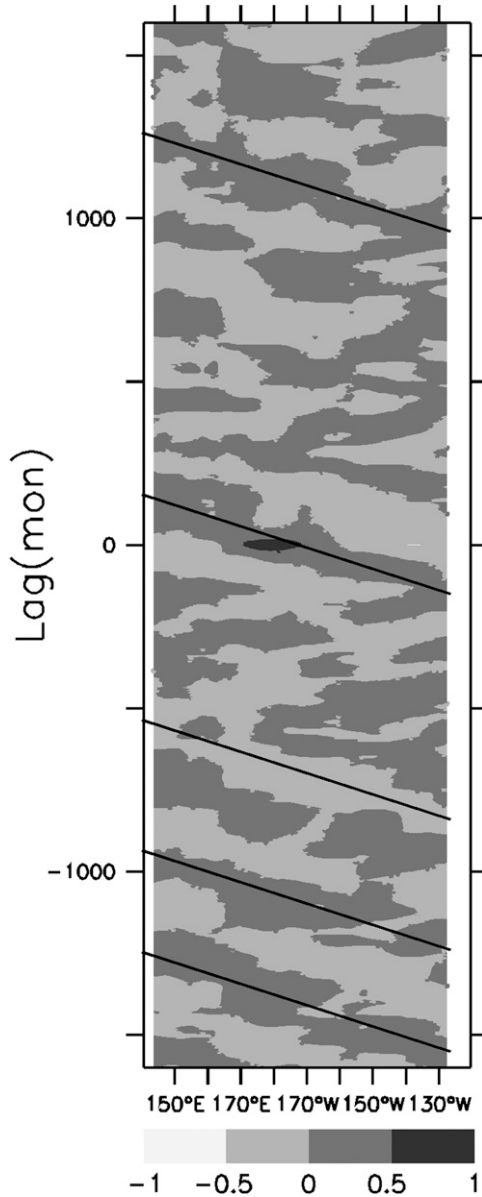
FIG. 16. ACF of monthly SSH anomalies at 50°N, with a base point of 180°E. The westward propagation of SSH anomalies is indicated with tilting lines.
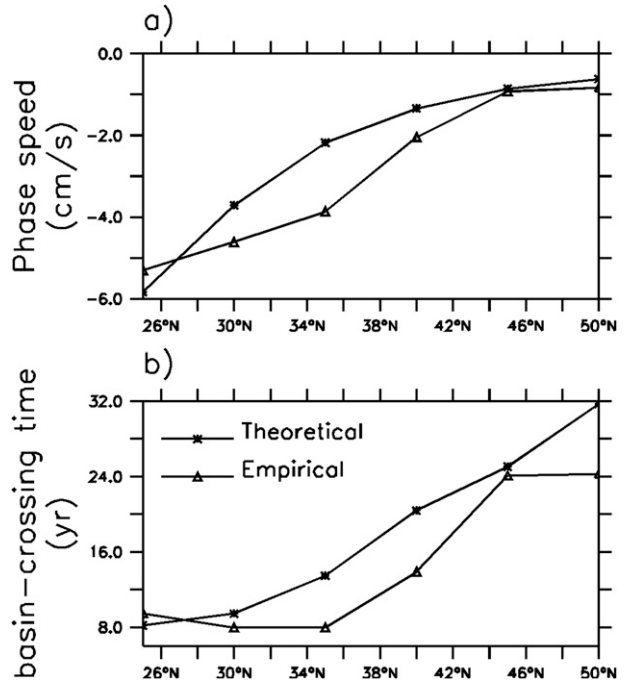

FIG. 17. (a) Phase speed of the first baroclinic-mode Rossby wave in the North Pacific and (b) the transmit time for the first baroclinic-mode Rossby wave to cross the North Pacific basin, based on theoretical (stars) and empirical (triangles) estimates.

and northern KOE. This yields an effective positive feedback for the multidecadal variability when combined with the mean halocline stratification.

This novel mechanism of PMV takes the form of a delayer oscillator, in essence. The wave adjustment in the subpolar North Pacific via propagating Rossby waves provides the delayed negative feedback, with the temperature–salinity convective feedback being the positive feedback. It differs fundamentally from other forms of delayer oscillators, including the midlatitude

coupled mode for PDV and the thermohaline-driven North Atlantic multidecadal variability. For the PDV, the delayed negative feedback arises from the meridional shift of the boundary between the subtropical and subpolar gyres as a response to wind curl forcing over the midlatitudes. For the North Atlantic multidecadal variability, the meridional advection associated with the deep thermohaline circulation acts as the delayed negative feedback. We have examined the possibility of a similar mechanism in the Pacific basin. The climatological meridional streamfunction of the North Pacific Ocean in the model is a shallow salinity-dominated cell (Winton and Sarachik 1993) confined to the upper 1000 m, with the sinking branch in the subtropics (not shown). Furthermore, there is no indication of a significant multidecadal oscillation in any portion of the meridional streamfunction.

One relevant example of decadal or multidecadal climate variability in nature was observed in the mid-to-late 1970s over the Pacific basin (e.g., Graham 1994; Miller et al. 1994; Trenberth and Hurrel 1994; Deser et al. 1996; Zhang and Levitus 1997). We attempt to compare the model simulation to observations regarding evolution of the anomaly fields and SST–SSS relationship, which are the key elements of our mechanism of PMV. However, this observed regime shift might have resulted
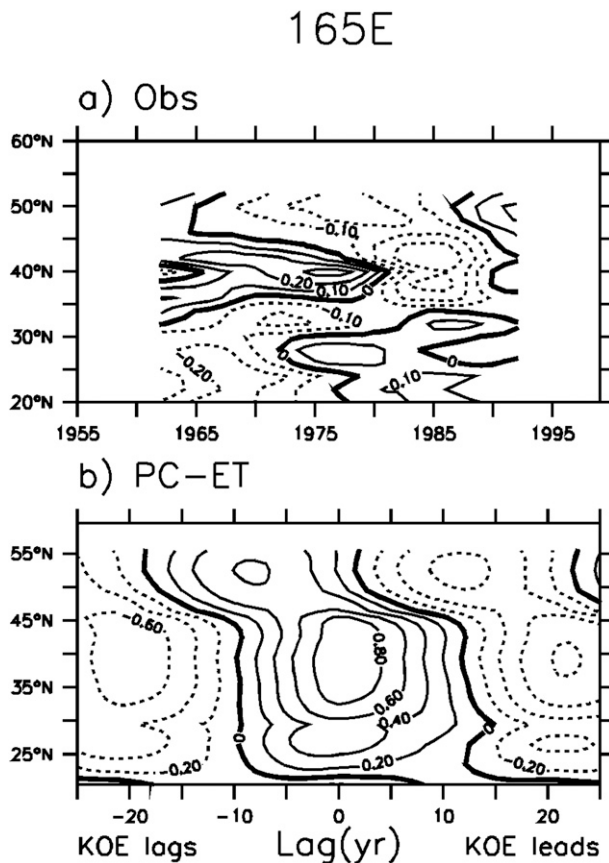
FIG. 18. Hovmöller diagram of SST evolution along 165°E. (a) The 15-yr low-pass-filtered SST anomaly (°C) during the second half of twentieth century, based on XBT observations. (b) Lagged correlation of SST upon SST in the KOE from PC-ET simulation. A 25–80-yr band filter is applied before calculation of correlation coefficients.

from the simultaneous phase reversals of pentadecadal and bidecadal modes (Minobe 1999), which may complicate our model–observation comparison focusing on multidecadal (or pentadecadal) time scales. Most previous studies reported that the decadal SST variability in the KOE could be traced back to the central North Pacific (Seager et al. 2001; Schneider et al. 2002) or the subtropical latitudes (Zhang and Levitus 1997; Wu et al. 2005); whereas some other studies suggested that the subpolar North Pacific is also a plausible source (Miller and Schneider 2000; Auad 2003). Based on XBT observations of ocean temperature fields (Levitus and Boyer 1994), Fig. 18a shows that a cold anomaly first occurred in the subpolar region in the late 1960s. It then propagated southward to the KOE and possibly initiated the regime shift from warm to cold phase in the late 1970s, which is consistent with the result from the model simulation (Fig. 18b). Using the Simple Ocean Data Assimilation (SODA) reanalysis product (Carton et al. 2000), we ex-

amined the evolution of the salinity anomaly and its relationship with the temperature anomaly. Unlike the model simulation, no hint of synchronous temperature–salinity variability is found for the SODA product. The discrepancy indicates that the physics of SODA reanalysis system differ fundamentally from those of the CCSM3. Lack of in situ salinity observations in the 1970s makes it impossible to evaluate the model performance in simulating salinity variability associated with the PMV for the present day.

Therefore, a caveat of the present study is that this mechanism of PMV may be model dependent. Because of the paucity and short duration of the observational records, it is difficult to verify some key processes in the nature. Nevertheless, the framework of this mechanism has some implications for understanding the PMV in reality. For instance, it suggests the subpolar North Pacific may contribute to the generation of Pacific low-frequency variability and thus calls for a better observation and improved understanding of the physics occurring there.

A central issue of low-frequency variability is the role of large-scale air–sea interaction. A number of previous studies suggested the low-frequency variability in the ocean results from pure stochastic atmospheric forcing (e.g., Hasselmann 1976; Frankignoul et al. 1997; Jin 1997; Saravanan and McWilliams 1997). In some other studies, the oceanic feedback to atmosphere was found to be an indispensable link of the midlatitude coupled mode (Latif and Barnett 1994; Weng and Neelin 1999; Kwon and Deser 2007; Qiu et al. 2007). So far, there is no consensus on the role of atmosphere–ocean coupling.

Concerning the PMV in the discussion, it has been demonstrated that the KOE SST is able to force a large-scale atmospheric response that helps to generate the PMV. Even though the atmospheric response to midlatitude oceanic variability is modest compared to energetic atmospheric internal variability, it has been pointed out that atmospheric response is of increasing significance with longer time scales, because of the dramatic reduction of atmospheric internal variability (Kushnir et al. 2002; Liu et al. 2007). A related study of Kwon and Deser (2007) has demonstrated that in CCSM2 the magnitude of wind curl response is 60% as large as that of wind curl forcing at a decadal time scale. To evaluate significance of the wind curl response in the present model, we compare it to the forcing at a multidecadal time scale. It is known that the atmosphere adjusts to midlatitude SST forcing in about one month (Czaja and Frankignoul 2002). However, to preclude the effect of atmospheric forcing on SST, we use lag regression rather than simultaneous regression in assessing the magnitude of atmospheric response, because the atmosphere at a later time cannot impact the SST at a

previous time. To take into account the SST degeneration in 1 yr, we divide the response pattern (Fig. 6a) by the 1-yr SST degeneration rate (~ 0.6) and further scale it by the ratio of the standard deviation of multidecadal SST to that of unfiltered SST in the KOE (~ 0.5). The result shows that the wind curl response is 35% as strong as the wind curl forcing (Fig. 6b) over the subpolar North Pacific, and it is therefore potentially important for the multidecadal variability. However, it remains uncertain as to what extent this oceanic feedback affects the PMV. It may be critical to the generation of the PMV; or, it merely provides a positive feedback that modifies an intrinsic ocean mode (e.g., Cessi and Primeau 2001; Yang and Liu 2003; Delworth et al. 1993; Delworth and Greatbatch 2000; Griffies and Tziperman 1995; Selten et al. 1999; Huck et al. 1999; Colin de Verdière and Huck 1999). To gain further insight, well-designed experiments using an ocean-only model are required; yet, this is beyond the scope of this study.

Finally, historical studies have indicated that the PMV may have mixed origins involving complex feedbacks (Jin 1997; Neelin and Weng 1999; Schneider and Cornuelle

2005). In the present work, we have illustrated a plausible mechanism for the PMV in CCSM3. Yet, there remains much work to further validate this mechanism and evaluate its significance in the generation of the PMV in CCSM3.

APPENDIX

Covariance Functions of Surface Heat Flux and SST in a Simple Stochastic SST Model

It is heuristic to explore the relationship of surface heat flux and SST in terms of the simple stochastic SST
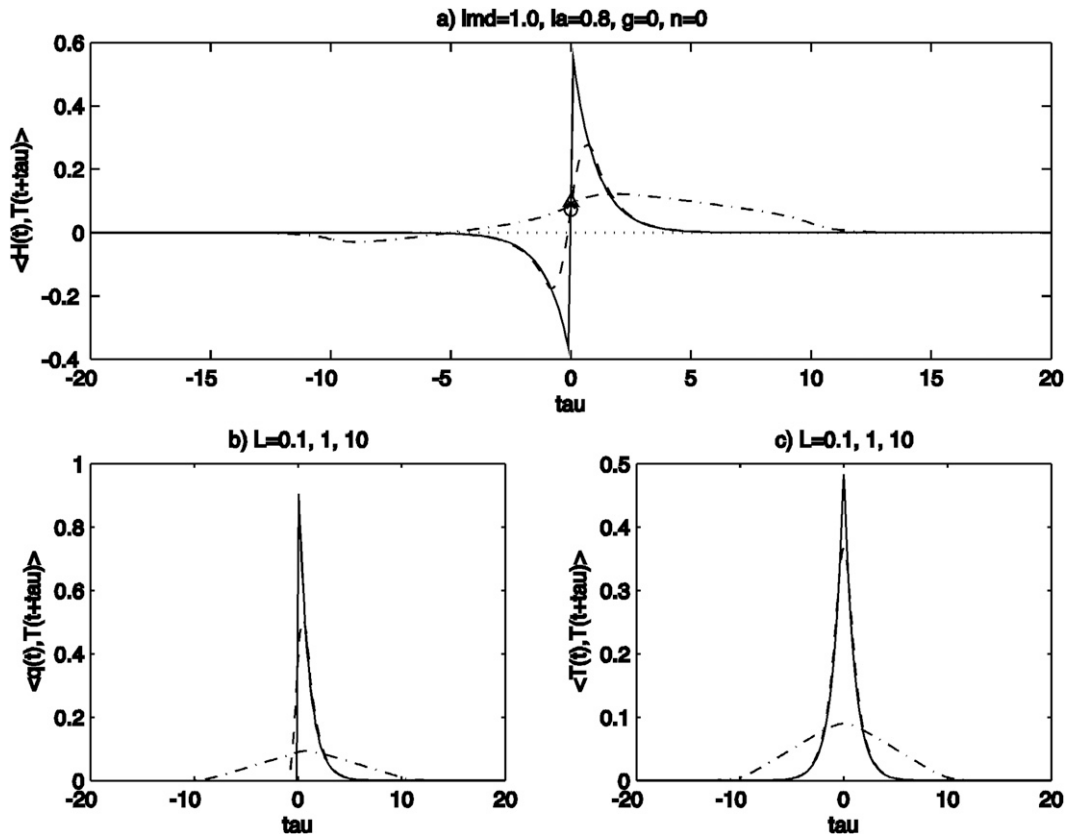

FIG. A1. Covariance of (a) T and H, (b) T and q, and (c) T for $\lambda = 1$, $\lambda_a = 0.8$, $\gamma = 0$, $n = 0$, and $\sigma = 1$. For solid, dashed, and dashed–dotted lines, $L = 0.1$, 1, and 10, respectively. Positive (negative) τ indicates T leading (lagging). Instantaneous covariance of T and H in (a) is highlighted with a triangle, circle, and star for $L = 0.1$, 1, and 10, respectively. For better visual effect, the covariance of T and H is multiplied by 5 for $L = 10$.

a) lmd=1.0, la=0.8, g=0, n=1
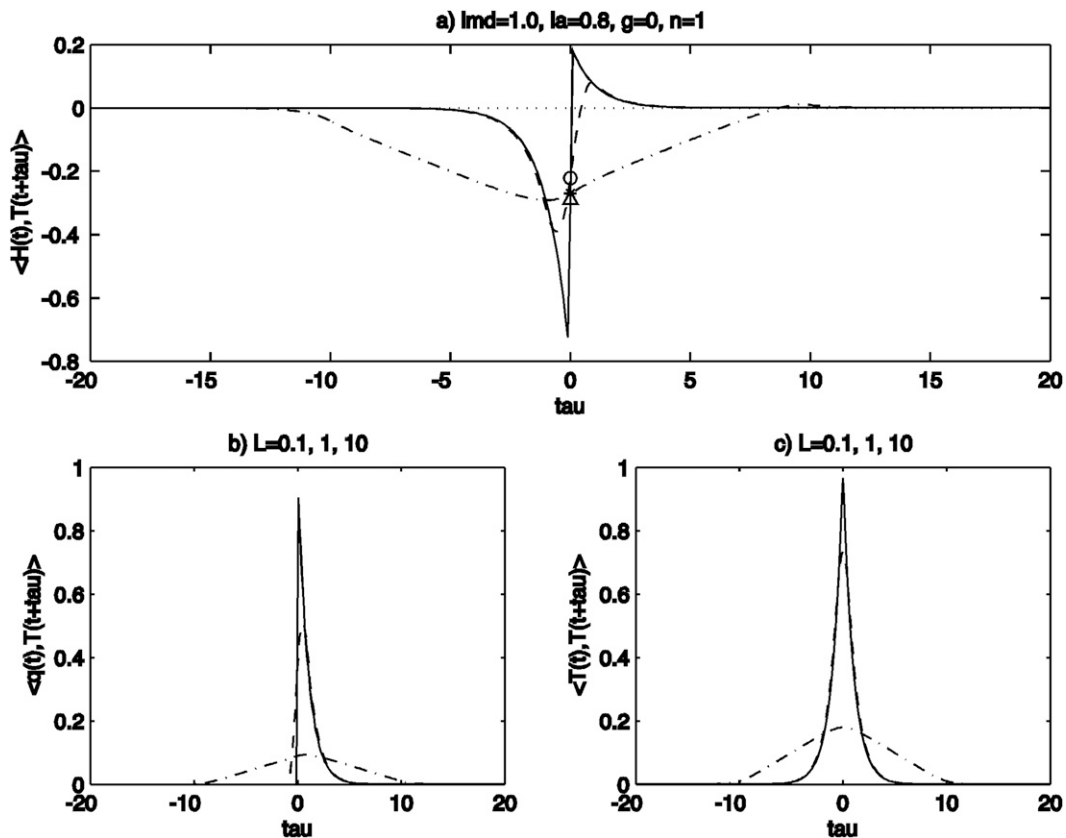
b) L=0.1, 1, 10

c) L=0.1, 1, 10

FIG. A2. As in Fig. A1, but for $n = 1$.

model proposed by Frankignoul et al. (1998). The SST equation takes the form

$$\partial_t T = H + m - \lambda_0 T, \qquad (A1)$$

where

$$H = q - \lambda_a T \qquad (A2)$$

is the surface heat flux, consisting of the stochastic forcing component q and the deterministic component resulting from SST feedback with λ_a being the heat flux feedback factor; m represents the other stochastic forcing terms, including those associated with wind stress changes, oceanic eddies, and teleconnection; and λ_0 represents all the contributions to the feedback that are not included in H.

For convenience, q and m are assumed to represent first-order Markov processes with a decay rate much

faster than $\lambda = \lambda_a + \lambda_0$, a variance ratio of n^2, and a correlation γ. Thus, T is given by

$$T = \int_{-\infty}^t e^{-\lambda(t-\tau)} f(\tau)\, d\tau, \qquad (A3)$$

where $f = m + q$. Given q variance of σ^2 and m variance of $n^2\sigma^2$, f can be shown to have variance of $\sigma_t^2 = \sigma^2(1 + 2\gamma n + n^2)$.

If we denote the average of a variable Z over a time period L by $\overline{Z}$, then

$$\overline{Z} = \frac{1}{L}\int_{-L/2}^{L/2} Z(t)\, dt, \qquad (A4)$$

and the covariance of the averaged SST anomaly, given that the decay time of q and m is much shorter than τ, becomes

$$\langle \overline{T}(t), \overline{T}(t + \tau)\rangle = \frac{2\sigma_t^2}{\lambda^3 L^2} sh^2\left(\frac{\lambda L}{2}\right) e^{-\lambda|\tau|}, \quad \text{for} \quad |\tau| \geq L, \quad \text{and}$$

$$= \frac{\sigma_t^2}{\lambda^3 L^2}[\lambda(L - |\tau|) + e^{-\lambda L}(ch(\lambda|\tau|) - e^{\lambda(L-|\tau|)})], \quad \text{for} \quad |\tau| < L. \qquad (A5)$$
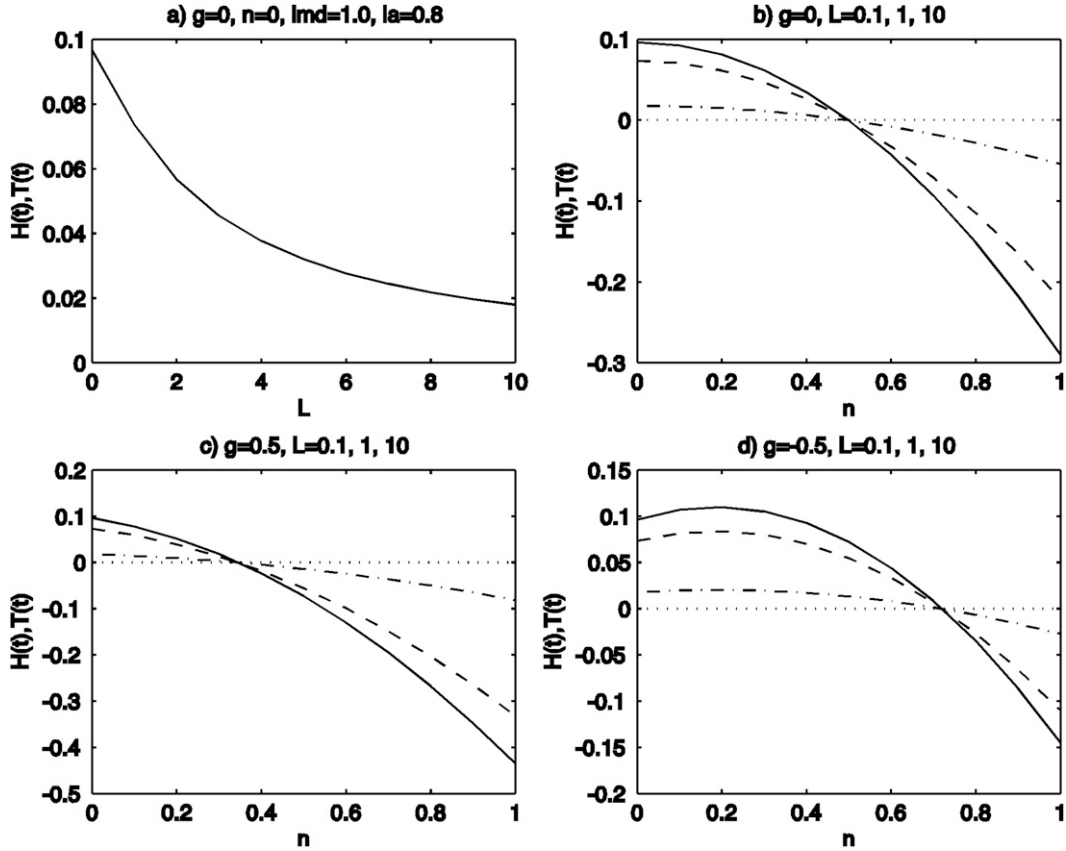
FIG. A3. Instantaneous covariance between T and H (a) as a function of L for $\lambda = 1, \lambda_a = 0.8, \gamma = 0, n = 0$, and $\sigma = 1$, and (b) as a function of n for $\lambda = 1, \lambda_a = 0.8, \gamma = 0$, and $\sigma = 1$. For solid, dashed, and dashed–dotted lines, $L = 0.1, 1$, and 10, respectively. (c) As in (b), but for $\gamma = 0.5$. (d) As in (b), but for $\gamma = -0.5$.

Similarly, the covariance between averaged T and q is found to be

$$\langle \overline{q}(t), \overline{T}(t+\tau) \rangle = 0, \quad \text{for} \quad \tau \le -L;$$

$$= \frac{\sigma^2(1+\gamma n)}{\lambda^2 L^2}[\lambda(L+\tau) - 1 + e^{-\lambda(L+\tau)}], \quad \text{for} \quad -L < \tau \le 0;$$

$$= \frac{\sigma^2(1+\gamma n)}{\lambda^2 L^2}[\lambda(L-\tau) + 1 - 2e^{-\lambda\tau} + e^{-\lambda(L+\tau)}], \quad \text{for} \quad 0 < \tau \le L; \quad \text{and}$$

$$= \frac{\sigma^2(1+\gamma n)}{\lambda^2 L^2}(e^{\lambda\tau} + e^{-\lambda\tau} - 2)e^{-\lambda\tau}, \quad \text{for} \quad \tau > L. \tag{A6}$$

Using (A2), the covariance between averaged T and H,

$$\langle \overline{H}(t), \overline{T}(t+\tau) \rangle = \langle \overline{q}(t), \overline{T}(t+\tau) \rangle$$
$$- \lambda_a \langle \overline{T}(t), \overline{T}(t+\tau) \rangle, \tag{A7}$$

can be readily obtained from (A5) and (A6), with the first term of right hand representing stochastic surface heat flux forcing on the SST and the second term representing the damping effect by SST-induced surface heat flux.

Here, we briefly discuss the dependence of the covariance between T and H on the parameters $\lambda, \lambda_a, L, \gamma$, and n. For instructive purposes, we first examine a simple case of $n = 0$ (i.e., the SST is purely driven by surface heat flux). Figure A1 plots the terms of (A7) as a function of τ and L, given standard parameters $\lambda = 1$, $\lambda_a = 0.8$, and $\sigma = 1$. For small L (relative to λ^{-1}; e.g., $L = 0.1$ or 1), the covariance between T and H is characterized by a strong asymmetry with positive maximum at T lagging and negative maximum at T leading. Physically,
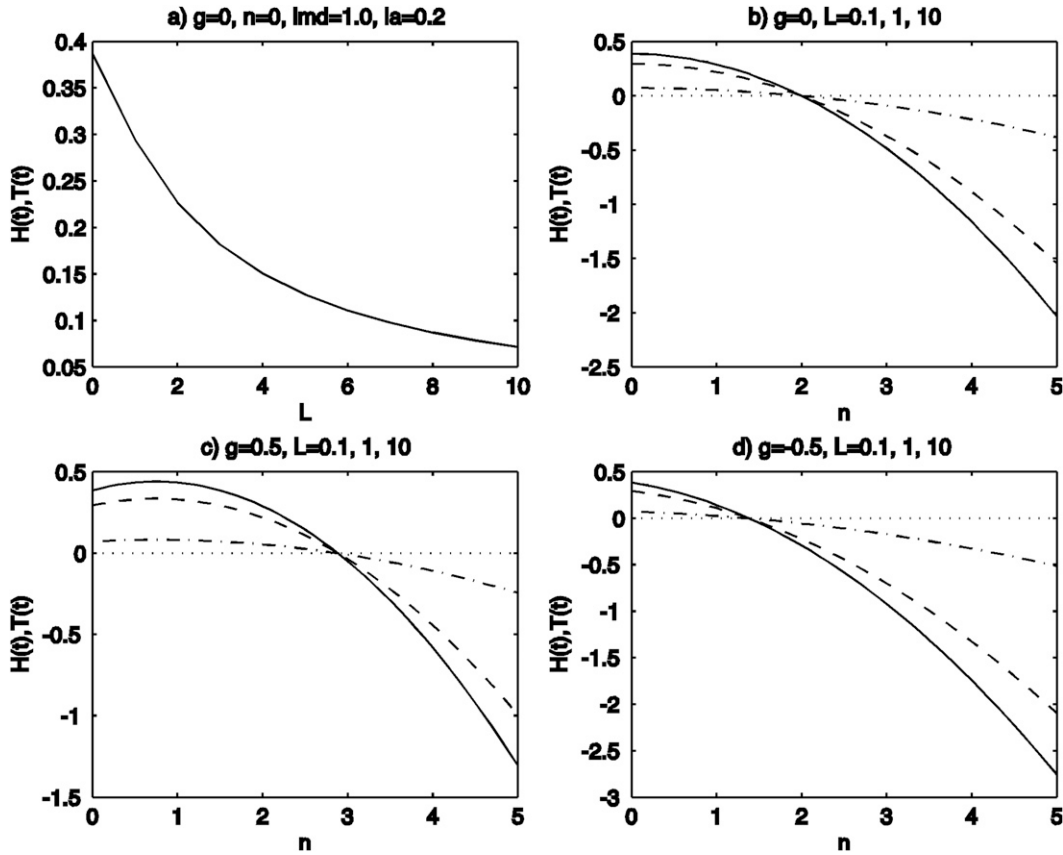
FIG. A4. As in Fig. A3, but for $\lambda = 1$ and $\lambda_a = 0.2$.

T responds to stochastic heat flux forcing (see Fig. A1b at T lagging) and induces additional surface heat flux (Fig. A1c at T leading). For large L (e.g., $L = 10$), the associated smoothing acts to attenuate the asymmetry in the covariance between T and q and hence that between T and H. Note that the instantaneous covariance ($\tau = 0$) between T and H always has a positive value regardless of L, as shown mathematically:

$$\langle \overline{H}(t), \overline{T}(t) \rangle = \frac{\sigma^2}{\lambda^2 L^2} [e^{-\lambda L} - (1 - \lambda L)]$$
$$\times [\underset{(1)}{(1 + \gamma n)} - \underset{(2)}{\frac{\lambda_a}{\lambda} (1 + 2\gamma n + n^2)}], \quad \text{(A8)}$$

$$= \frac{\sigma^2}{\lambda^2 L^2} [e^{-\lambda L} - (1 - \lambda L)]$$
$$\times \left[1 - \frac{\lambda_a}{\lambda} (1 + n^2) + \gamma n \left(1 - \frac{2\lambda_a}{\lambda} \right) \right], \quad \text{(A9)}$$

$$= \frac{\sigma^2}{\lambda^2 L^2} [e^{-\lambda L} - (1 - \lambda L)](1 - \frac{\lambda_a}{\lambda}) \succ 0,$$
$$\text{as } n = 0. \quad \text{(A10)}$$

So the T always has a positive instantaneous correlation with H, with or without smoothing, when it is purely driven by surface heat flux. A negative instantaneous correlation thus implies a direct oceanic source for the SST variability.

Indeed, the instantaneous covariance between T and H is found to be negative in the case of $n = 1$ and $\gamma = 0$ (i.e., the SST variability has another source that is distinct from the surface heat flux; Fig. A2). The covariance between T and q [term 1 of (A8)] remains identical to that in previous case. The change consists in the term associated with SST-induced surface flux [term 2 of (A8)], which becomes larger because of the additional source for SST variability. Consequently, the total heat flux H has a negative instantaneous correlation with the SST for its predominant damping effect rather than a driving force for the SST variability.

Figure A3 plots the instantaneous covariance between T and H as a function of L, n and γ. Again, when the SST is driven purely by surface heat flux ($n = 0$), the instantaneous covariance decreases with larger L and yet remains positive. When another source for the SST variability exists ($n > 0$), the instantaneous covariance

likely becomes negative as long as the additional source is sufficiently strong. As inferred from (A9), the critical magnitude n_c depends on parameter γ, the relationship of the additional source and surface heat flux. For typical parameters $\lambda = 1$ and $\lambda_a = 0.8$, more positive (negative) γ makes the covariance more negative (positive), and hence the n_c is smaller (larger). For example, $n_c = 0.3, 0.5$, and 0.7 for $\gamma = 0.5, 0$, and -0.5, respectively. Specifically, the increase (decrease) in the covariance between T and q [term 1 of (A8)] is smaller than that in the term associated with SST-induced surface flux [term 2 of (A8)], in response to an additional source that is positively (negatively) correlated with the surface heat flux. Conversely, for $\lambda = 1$ and $\lambda_a = 0.2$ (Fig. A4), more positive (negative) γ results in larger (larger) n_c, because the change in covariance between T and q predominates over that associated with SST-induced surface heat flux. In contrast, the n_c is much larger here than for $\lambda = 1$ and $\lambda_a = 0.8$.

REFERENCES

Arzel, O., T. Huck, and A. Colin De Verdière, 2006: The different nature of the interdecadal variability of the thermohaline circulation under mixed and flux boundary conditions. *J. Phys. Oceanogr.,* **36,** 1703–1718.

Auad, G., 2003: Interdecadal dynamics of the North Pacific Ocean. *J. Phys. Oceanogr.,* **33,** 2483–2503.

Barsugli, J. J., and D. S. Battisti, 1998: The basic effects of atmosphere–ocean thermal coupling on midlatitude variability. *J. Atmos. Sci.,* **55,** 477–493.

Carton, J. A., G. Chepurin, and X. Cao, 2000: A simple ocean data assimilation analysis of the global upper ocean 1950–95. Part II: Results. *J. Phys. Oceanogr.,* **30,** 311–326.

Cessi, P., and F. Primeau, 2001: Dissipative selection of low-frequency modes in a reduced-gravity basin. *J. Phys. Oceanogr.,* **31,** 127–137.

Chelton, D. B., and M. G. Schlax, 1996: Global observations of oceanic Rossby waves. *Science,* **272,** 234–238.

——, R. A. DeSzoeke, M. G. Schlax, K. E. Naggar, and N. Siwertz, 1998: Geographical variability of the first baroclinic Rossby radius of deformation. *J. Phys. Oceanogr.,* **28,** 433–460.

Colin de Verdière, A., and T. Huck, 1999: Baroclinic instability: An oceanic wavemaker for interdecadal variability. *J. Phys. Oceanogr.,* **29,** 893–910.

Collins, W. D., and Coauthors, 2006: The Community Climate System Model version 3 (CCSM3). *J. Climate,* **19,** 2122–2143.

Cooper, N. S., 1988: The effect of salinity on tropical ocean models. *J. Phys. Oceanogr.,* **18,** 697–707.

Czaja, A., and C. Frankignoul, 2002: Observed impact of Atlantic SST anomalies on the North Atlantic oscillation. *J. Climate,* **15,** 606–623.

Delworth, T. L., and R. J. Greatbatch, 2000: Multidecadal thermohaline circulation variability driven by atmospheric surface flux forcing. *J. Climate,* **13,** 1481–1495.

——, S. Manabe, and R. J. Stouffer, 1993: Interdecadal variations of the thermohaline circulation in a coupled ocean–atmosphere model. *J. Climate,* **6,** 1993–2011.

Deser, C., M. A. Alexander, and M. S. Timlin, 1996: Upper-ocean thermal variations in the North Pacific during 1970–1991. *J. Climate,* **9,** 1840–1855.

——, A. S. Phillips, and J. W. Hurrell, 2004: Pacific interdecadal climate variability: Linkages between the tropics and the North Pacific during boreal winter since 1900. *J. Climate,* **17,** 3109–3124.

d'Orgeville, M., and W. R. Peltier, 2007: On the Pacific Decadal Oscillation and the Atlantic Multidecadal Oscillation: Might they be related? *Geophys. Res. Lett.,* **34,** L23705, doi:10.1029/2007GL031584.

Eden, C., and J. Greatbatch, 2003: A damped decadal oscillation in the North Atlantic climate system. *J. Climate,* **16,** 4043–4060.

Enfield, D. B., and A. M. Mestas-Nunez, 1999: Multiscale variabilities in global sea surface temperatures and their relationships with tropospheric climate patterns. *J. Climate,* **12,** 2719–2733.

Frankignoul, C., P. Muller, and E. Zorita, 1997: A simple model of the decadal response of the ocean to stochastic wind forcing. *J. Phys. Oceanogr.,* **27,** 1533–1546.

——, A. Czaja, and B. L'Heveder, 1998: Air–sea feedback in the North Atlantic and surface boundary conditions for ocean models. *J. Climate,* **11,** 2310–2324.

Graham, N. E., 1994: Decadal-scale climate variability in the tropical and North Pacific during the 1970s and 1980s: Observations and model results. *Climate Dyn.,* **10,** 135–162.

Griffies, S. M., and E. Tziperman, 1995: A linear thermohaline oscillator driven by stochastic atmospheric forcing. *J. Climate,* **8,** 2440–2453.

Hasselmann, K., 1976: Stochastic climate models. 1. Theory. *Tellus,* **28,** 473–485.

Huck, T., A. Colin de Verdière, and A. J. Weaver, 1999: Interdecadal variability of the thermohaline circulation in box-ocean models forced by fixed surface fluxes. *J. Phys. Oceanogr.,* **29,** 865–892.

Jacobs, G. A., and J. L. Mitchell, 1996: Ocean circulation variations associated with the Antarctic Circumpolar Wave. *Geophys. Res. Lett.,* **23,** 2947–2950.

Jin, F. F., 1997: A theory of interdecadal climate variability of the North Pacific ocean–atmosphere system. *J. Climate,* **10,** 1821–1835.

Kleeman, R., J. P. McCreary, and B. A. Klinger, 1999: A mechanism for generating ENSO decadal variability. *Geophys. Res. Lett.,* **26,** 1743–1746.

Kushnir, Y., W. A. Robinson, I. Blade, N. M. J. Hall, S. Peng, and R. Sutton, 2002: Atmospheric GCM response to extratropical SST anomalies: Synthesis and evaluation. *J. Climate,* **15,** 2233–2256.

Kwon, Y., and C. Deser, 2007: North Pacific decadal variability in the Community Climate System Model version 2. *J. Climate,* **20,** 2416–2433.

Landerer, F. W., J. H. Jungclaus, and J. Marotzke, 2007: Regional dynamic and steric sea level change in response to the IPCC-A1B scenario. *J. Phys. Oceanogr.,* **37,** 296–312.

Latif, M., 2006: On North Pacific multidecadal climate variability. *J. Climate,* **19,** 2906–2915.

——, and T. P. Barnett, 1994: Causes of decadal climate variability over the North Pacific and North America. *Science,* **266,** 634–637.

——, and ——, 1996: Decadal climate variability over the North Pacific and North America: Dynamics and predictability. *J. Climate,* **9,** 2407–2423.

Lenderink, G., and R. J. Haarsma, 1994: Variability and multiple equilibria of the thermohaline circulation associated with deep-water formation. *J. Phys. Oceanogr.,* **24,** 1480–1493.

Levitus, S., and T. P. Boyer, 1994: *Temperature.* Vol. 4, *World Ocean Atlas 1994,* NOAA Atlas NESDIS 4, 117 pp.

Liu, Z., 1999a: Planetary wave modes in thermocline circulation: Non-Doppler-shift mode, advective mode and Green mode. *Quart. J. Roy. Meteor. Soc.,* **125,** 1315–1339.

——, 1999b: Forced planetary wave response in a thermocline gyre. *J. Phys. Oceanogr.,* **29,** 1036–1055.

——, L. Wu, R. Gallimore, and R. Jacob, 2002: Search for the origins of Pacific decadal climate variability. *Geophys. Res. Lett.,* **29,** 1404, doi:10.1029/2001GL013735.

——, Y. Liu, L. Wu, and R. Jacob, 2007: Seasonal and long-term atmospheric responses to reemerging North Pacific Ocean variability: A combined dynamical and statistical assessment. *J. Climate,* **20,** 955–980.

Mann, M., and J. Lees, 1996: Robust estimation of background noise and signal detection in climate time series. *Climatic Change,* **33,** 409–445.

Mantua, N. J., S. R. Hare, Y. Zhang, J. M. Wallace, and R. C. Francis, 1997: A Pacific interdecadal climate oscillation with impacts on salmon production. *Bull. Amer. Meteor. Soc.,* **78,** 1069–1079.

Miller, A. J., and N. Schneider, 2000: Interdecadal climate regime dynamics in the North Pacific Ocean: Theories, observations and ecosystem impacts. *Prog. Oceanogr.,* **47,** 355–379.

——, D. R. Cayan, T. P. Barnett, N. E. Graham, and J. M. Oberhuber, 1994: Interdecadal variability of the Pacific Ocean: Model response to observed heat flux and wind stress anomalies. *Climate Dyn.,* **9,** 287–302.

Minobe, S., 1997: A 50–70 year climatic oscillation over the North Pacific and North America. *Geophys. Res. Lett.,* **24,** 683–686.

——, 1999: Resonance in bidecadal and pentadecadal climate oscillations over the North Pacific: Role in climatic regime shifts. *Geophys. Res. Lett.,* **26,** 855–858.

——, 2000: Spatio-temporal structure of the pentadecadal variability over the North Pacific. *Prog. Oceanogr.,* **47,** 381–408.

Neelin, J. D., and W. Weng, 1999: Analytical prototypes for ocean–atmosphere interaction at midlatitudes. Part I: Coupled feedbacks as a sea surface temperature dependent stochastic process. *J. Climate,* **12,** 697–721.

Pierce, D. W., T. P. Barnett, N. Schneider, R. Saravanan, D. Dommenget, and M. Latif, 2001: The role of ocean dynamics in producing decadal climate variability in the North Pacific. *Climate Dyn.,* **18,** 51–70.

Qiu, B., 2003: Kuroshio Extension variability and forcing of the Pacific decadal oscillations: Responses and potential feedback. *J. Phys. Oceanogr.,* **33,** 2465–2482.

——, N. Schneider, and S. Chen, 2007: Coupled decadal variability in the North Pacific: An observationally constrained idealized model. *J. Climate,* **20,** 3602–3620.

Rodwell, M. J., D. P. Rowell, and C. K. Folland, 1999: Oceanic forcing of the wintertime North Atlantic oscillation and European climate. *Nature,* **398,** 320–323.

Saravanan, R., and J. C. McWilliams, 1997: Stochasticity and spatial resonance in interdecadal climate fluctuations. *J. Climate,* **10,** 2299–2320.

Schneider, N., and B. D. Cornuelle, 2005: The forcing of the Pacific decadal oscillation. *J. Climate,* **18,** 4355–4373.

——, A. J. Miller, and D. W. Pierce, 2002: Anatomy of North Pacific decadal variability. *J. Climate,* **15,** 586–605.

Seager, R., Y. Kushnir, N. H. Naik, M. A. Cane, and J. Miller, 2001: Wind-driven shifts in the latitude of the Kuroshio–Oyashio Extension and generation of SST anomalies on decadal timescales. *J. Climate,* **14,** 4249–4265.

Selten, F. M., R. J. Haarsma, and J. D. Opsteegh, 1999: On the mechanism of North Atlantic decadal variability. *J. Climate,* **12,** 1956–1973.

Solomon, A., J. P. McCreary, R. Kleeman, and B. A. Klinger, 2003: Interannual and decadal variability in an intermediate coupled model of the Pacific region. *J. Climate,* **16,** 383–405.

Timmermann, A., M. Latif, R. Voss, and A. Grötzner, 1998: Northern Hemispheric interdecadal variability: A coupled air–sea mode. *J. Climate,* **11,** 1906–1931.

Trenberth, K. E., and J. W. Hurrel, 1994: Decadal atmosphere-ocean variations in the Pacific. *Climate Dyn.,* **9,** 303–319.

Weng, W. J., and J. D. Neelin, 1999: Analytical prototypes for ocean–atmosphere interaction at midlatitudes. Part II: Mechanisms for coupled gyre modes. *J. Climate,* **12,** 2757–2774.

Winton, M., and E. S. Sarachik, 1993: Thermohaline oscillations induced by strong steady salinity forcing of ocean general circulation models. *J. Phys. Oceanogr.,* **23,** 1389–1410.

Wu, L., Z. Liu, R. Gallimore, R. Jacob, D. Lee, and Y. Zhong, 2003: Pacific decadal variability: The tropical Pacific mode and the North Pacific mode. *J. Climate,* **16,** 1101–1120.

——, D. Lee, and Z. Liu, 2005: The 1976/77 North Pacific climate regime shift: The role of subtropical ocean adjustment and coupled ocean–atmosphere feedbacks. *J. Climate,* **18,** 5125.

Yang, H., and Z. Liu, 2003: Basin modes in a tropical–extratropical basin. *J. Phys. Oceanogr.,* **33,** 2751–2763.

Yeager, S. G., C. A. Shields, W. G. Large, and J. J. Hack, 2006: The low-resolution CCSM3. *J. Climate,* **19,** 2545–2566.

Zhang, R., and S. Levitus, 1997: Structure and cycle of decadal variability of upper-ocean temperature in the North Pacific. *J. Climate,* **10,** 710–727.

Zhong, Y., and Z. Liu, 2008: A joint statistical and dynamical assessment of atmospheric response to North Pacific oceanic variability in CCSM3. *J. Climate,* **21,** 6044–6051.

——, ——, and R. Jacob, 2008: Origin of Pacific multidecadal variability in Community Climate System Model, version 3 (CCSM3): A combined statistical and dynamical assessment. *J. Climate,* **21,** 114–133.